Analysis of Aging Severity Factors
For Automotive Lithium Ion Batteries

Undergraduate Honors Thesis

Presented in Partial Fulfillment of the Requirements for

Graduation with Distinction

at The Ohio State University

By

Alexander K. Suttman

* * * * *

The Ohio State University

2010

Defense Committee:

Professor Yann Guezennec, Advisor

Professor Stephen Yurkovich

Approved by

_____

Advisor

Undergraduate Program in Mechanical Engineering

ABSTRACT

As any battery is charged and recharged through its use, the maximum power and capacity of the battery slowly decrease. This phenomenon, termed ‘aging’, is of particular concern in fields such as the automotive industry where long battery life is essential,. Furthermore, this ‘aging’ is present with all battery chemistries. While the ‘aging’ can be traced back to a multiplicity of internal microscopic material degradation processes, the purpose of this project was to identify the macroscopic conditions under which batteries age most rapidly in order to predict or even extend useful battery life by avoiding these conditions. Specifically, this project focuses on advanced Li-ion batteries by identifying simplified electrical models of battery characteristics and tracking the slow evolution of the model parameters through the life of the battery. This analysis was performed for many batteries which underwent different conditions of aging (state of charge and current levels) and leverages several years of experiments at the Center for Automotive Research. The initial results indicate it is feasible to track this aging process by this methodology and that this aging process can be simply modeled by a slow dynamic model which depends on the severity of the operating conditions. Further, this approach could be performed in-situ in the vehicle with simple measurements readily available.

ACKNOWLEDGMENTS

I would like to thank Professor Guezennec for providing me with this project and for all of the support and advice he has given me over the past year. I would also like to thank John Neal and Dr. Simona Onori for answering any questions I had along the way.

TABLE OF CONTENTS

Page

LIST OF FIGURES

CHAPTER 1

INTRODUCTION

1.1 Introduction

According to a report issued by the Energy Information Administration, worldwide energy consumption is projected to expand by 50 percent from 2005 to 2030 and the United States alone consumes approximately 23% of this total [1]. As the need for energy continues to increase, so does the need for transporting and storing it. The most obvious solution for physically storing and transporting energy comes in a package that nearly every American deals with on a daily basis – batteries.

Batteries power a wide range of devices, from cell phones and laptops to pacemakers and hearing aids. The convenience of storing electricity and taking it with us wherever we go is undeniable. In the past decade, we have seen more and more emphasis being placed on the environment and decreasing our dependence on foreign oil. As a result, battery powered automobiles such as the Toyota Prius have become a common sight on the road today.

While hybrid electric vehicles may seem like standard technology on the road today, placing batteries in the dynamic environment of an automobile is still a demanding

task that presents a unique set of challenges. First of all, the performance demands placed on these batteries are much higher than in typical battery applications, with high levels of electric current charging and draining the battery. Also, these batteries are placed in a very harsh physical environment, subject to vibrations as well as high temperatures. It is because of these high levels of current and high temperature operating environment that batteries placed in hybrid electric vehicles suffer from accelerated aging.

Battery packs placed in hybrid electric vehicles are expensive and very labor intensive to replace, for this reason they must be designed to last for the life of the vehicle. Symptoms that arise from battery aging include the loss of rated capacity, faster temperature rise during operation, reduced charge acceptance, higher internal resistance, lower voltage, and more frequent self discharge [2]. In automotive applications we are primarily concerned with the increase of resistance which results in a loss of power, and is accompanied by a decrease of storage capacity. In order to design battery packs for maximum life, we need to develop an effective procedure that will allow us to not only measure the parameters that define these behaviors, but predict and ultimately delay their manifestation. The development of such a procedure will require extensive experimentation and analysis.

The research required to develop a suitable procedure for predicting aging severity is already taking place at the Center for Automotive Research. For the past 24 months, the center has operated multiple aging stations in its aging laboratory, collecting thousands of hours of data. The focus of the project described in this paper is in

analyzing this aging data and extracting useful information regarding the conditions under which batteries age, and the rate at which it occurs.

1.2 Literature Review

As battery technology moves forward, research into battery aging and battery pack management is required to support this advancement. Currently, a large amount of battery research is taking place at the Ohio State University Center for Automotive Research, particularly in the field of battery aging. This literature review will establish the need for the development of Lithium Ion batteries for use in hybrid electric vehicles, explore the concepts and challenges of battery modeling, and cover methods that have been developed for identifying battery models related to aging.

In *Batteries for Plug-In Hybride Electric Vehicles (PHEV's): Goals and the State of Technology circa 2008* [3], Axen et al. highlight the development of advanced batteries of different chemistries for hybrid vehicle applications. Due to cost, weight, and space constraints in vehicles, current production battery packs are made from nickel-metal hydride (NiMH) battery cells. They argue that compared to other battery chemistries currently in use, such as NiMH, Li-Ion and Li-Ion polymer battery chemistries have batter energy densities that better suited to meet the requirements of today's new hybrid vehicle technologies. However, despite the advantages of Li-Ion batteries, Axen warns that the technology is not yet firmly established for automotive applications and in order for development in this area to continue, issues such as longevity and safety must be addressed.

Battery lifetime is one of the largest barriers preventing widespread adoption of lithium ion battery chemistries in automotive, as well as stationary applications. Sauer and Wenzl explain that all battery systems are affected by a wide range of aging processes in *Comparison of different approaches for lifetime prediction of electrochemical systems* [4]. They explain that many of these processes occur due to different stress factors and operating conditions imposed on the battery. Some of these factors include the number of charging cycles a battery has experienced, the battery state of charge at which cycling occurs, frequency of battery operation, and wide ranges of temperatures during operation.

Because battery aging is difficult to analyze in a laboratory setting [5], the use of battery models is necessary to gain insight into the evolution of aging processes over the life of a battery. In the past decade, battery modeling and simulation has become much easier and less expensive to implement thanks to substantial improvements in computer power and software capability. Two approaches are used to model the behavior of a battery cell. The first type of modeling is known as fundamental, or particle-based distribution modeling. These models take the particle movement and chemical reactions of a battery into account using partial differential equations. They achieve high levels of accuracy but are very computationally demanding. Phenomenological models are the second method used to represent battery behavior. Instead of attempting to represent the fundamental physics of a system, these models provide a representation of the input/output relationship of the system. These models are much less complex from a mathematical standpoint, and are much simpler to solve in real time applications.

However, these models are not typically able to achieve accuracies as high as fundamental models.

Different types of phenomenological models exist for batteries, the most common is the equivalent circuit model. The equivalent circuit model is simple but it is capable of capturing battery dynamics under at different sets of battery operating conditions. This characteristic makes it attractive for use with model based estimation techniques in automotive applications.

In Electro-Thermal Battery Modeling and Identification for Automotive Applications [6], Hu et al. describe a methodology for modeling and identifying dynamic behavior of batteries using such an equivalent circuit model. This equivalent circuit model representation is known as the standard Randle equivalent circuit, comprised of an ideal voltage source, an internal resistance, and *n* parallel RC circuits, where the value of *n* is the order of the model. The values of circuit elements contained in these models are non constant functions dependent on temperature, state of charge, and current direction. Hu et al. note that while this is not the most sophisticated battery model possible, it is often selected because of its simplicity and universality. It is for these reasons that the Randle equivalent circuit was chosen as the primary vehicle of model based analyses in this project.

Hu et al. go on to detail a method for battery model identification in which the values of electrical circuit elements contained in the equivalent circuit model are identified. This is accomplished by generating a simulated model voltage with a guessed

set of initial values, and then optimizing the model coefficients to minimize the difference between the modeled battery voltage and the measured battery voltage under identical current patterns. This method of optimization was also adopted for use in this project.

1.3 Motivation

From the literature, established and accepted models have been developed to identify battery model parameters. By performing this identification at many points in the life of a battery, we can gain an understanding of which battery operating conditions contribute to accelerated rates of aging. Although this exercise has been applied in the past, this project aims to take advantage of previously collected data that is otherwise of no use. This project will be successful if we are able to extract useful information regarding battery aging from data that was not intended for this purpose.

1.4 Project Objective

The goal of this project is to study these existing data sets, learn the modeling and identification techniques that are required to analyze them, and use this analysis to identify important aging parameters. These aging parameters could come in the form of severity factors, or similar methods of rating the impact certain operating conditions have on the rate of battery aging.

CHAPTER 2

METHODOLOGY

2.1 Data Collection

As mentioned previously, the data set considered in this project was collected at the OSU Center for Automotive Research (CAR). This data collection took place in the CAR battery aging lab, created in 2008. The aging lab contained a number of battery aging set ups, all carefully monitored and protected by fire control systems. The data set used in this experiment was collected from March 2008 through April 2009 on three separate aging stations. The aging regimen itself consisted of capacity tests, pulse tests, cold start tests, and aging cycles of different types performed in a prescribed order.

These battery aging experiments sometimes required high voltages and large currents to be passed in and out of the batteries. This action produced large amounts of heat which, if not carefully monitored, could result in fire. To reduce the risk of fire, the aging lab was equipped with a number of safety measures. Each battery controller was programmed to cut off power to a battery if voltage moved outside a predetermined set of upper and lower bounds. This ensured that if a battery failed, power was cut off. Additionally, each aging station was fitted with an emergency stop button to cut power

manually to a given station. A second emergency cutoff switch existed to cut off power to the entire aging lab. In the event that the aging lab was not staffed when a problem occurred, smoke detectors were programmed to contact the local fire department and send text message and email alerts to the aging lab supervisor. Twenty-four hour video surveillance allowed the lab to be monitored from any computer with an internet connection, and regular email updates on the status of each battery were set up as well.

Aging stations were contained in electrical equipment racks, with 2 stations occupying a single rack as seen in Figure 1. A single station was comprised of a battery, a battery load, a power supply, and a controller. The battery load and power supply were purchased from AMREL and are pictured in Figure 2. Each battery was contained inside of a Peltier junction, a type of thermoelectric heat pump, to regulate its temperature.

Like the fire control systems, the repetitive nature of these aging regimens required that they be highly automated. T accomplish this, each AMREL battery load was controlled by a small form factor PC running Matlab. Separate Matlab scripts were programmed for each of the aging tests mentioned earlier, and an individual battery underwent only a single aging test protocol each day. These PCs were also responsible for data collection. Data was collected at a rate of 10 hertz and measurements included time, current, voltage, and temperature. Once data was collected, it was backed up on optical media for storage.

Figure 1: OSU Center for Automotive Research Battery Aging Lab

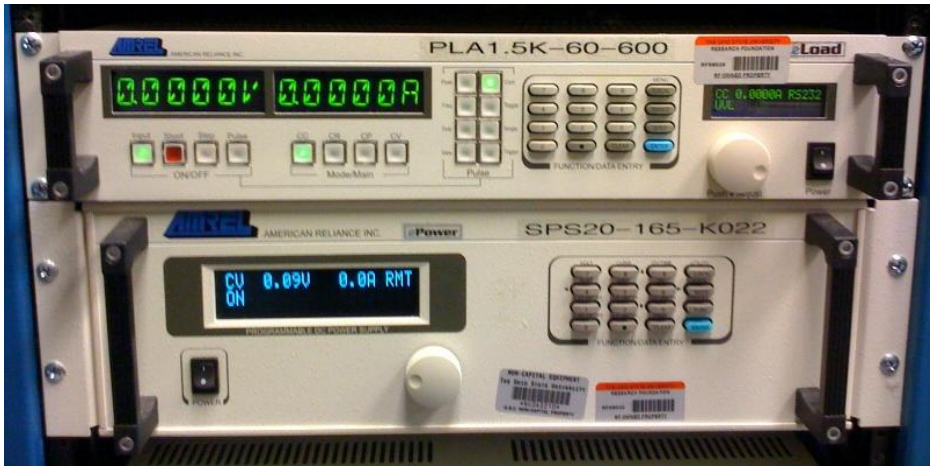

Figure 2: AMREL battery supply / load pair

A typical battery aging regimen consisted of a number of tests and trials, including capacity tests, pulse tests, cold start tests, and aging cycles. In between every test, batteries were reset to their prescribed charge level as well. Performing a capacity test on a battery consisted of charging the battery to 100% state of charge (SOC), then discharging the battery at a current rate of 1C until battery voltage reached a lower limit. State of charge is a measure of the battery's remaining capacity expressed as a percentage of its total capacity. A current rate of 1C refers to a current level that will completely discharge the battery in one hour, A current rate of 2C would drain a battery in half an hour, and so on. This full charge and discharge was repeated multiple times for each capacity test as seen below in Figure 3

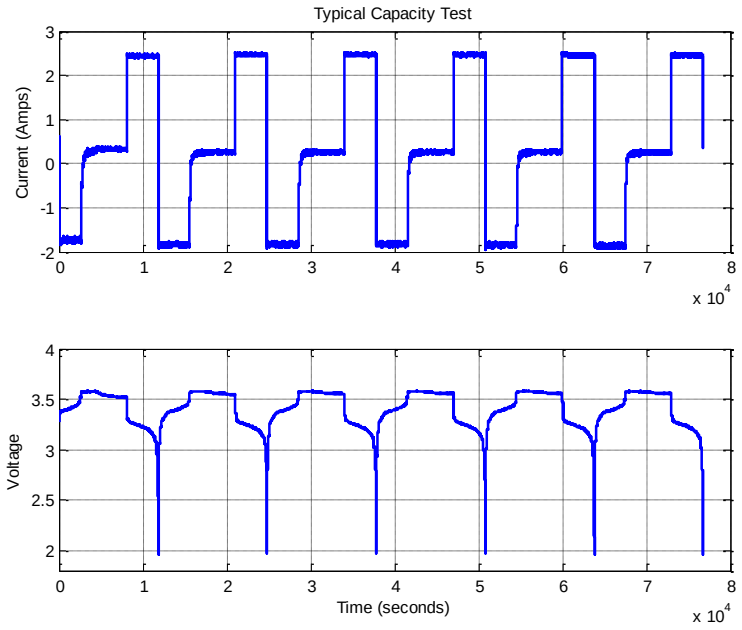

Figure 3: Typical Capacity Test

Pulse testing procedures were derived from the hybrid pulse power characterization test process outlined in Freedom Car Battery Test Manual for Power-Assist Hybrid Electric Vehicles [8]. In a typical pulse test, the battery was subjected to a series of increasing 10 second current bursts. Pulse tests measured the battery's ability to respond to large but short current demands. A typical pulse test is pictured in Figure 4.

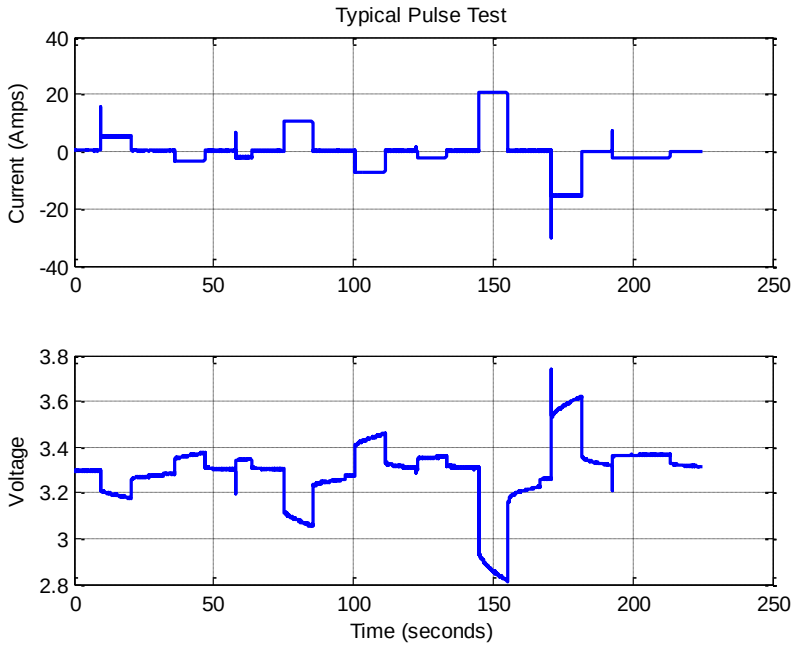

Figure 4: Typical Pulse Test

Cold start tests were performed on batteries as well, although less frequently than other tests. Cold start test procedures were derived from Freedom Car Battery Test Manual for Power-Assist Hybrid Electric Vehicles. These tests required the battery to be placed in an extremely low temperature environment (-20°C) and discharged in 30 second bursts with 2 minutes between discharges. An example of a cold start test is pictured in Figure 5.

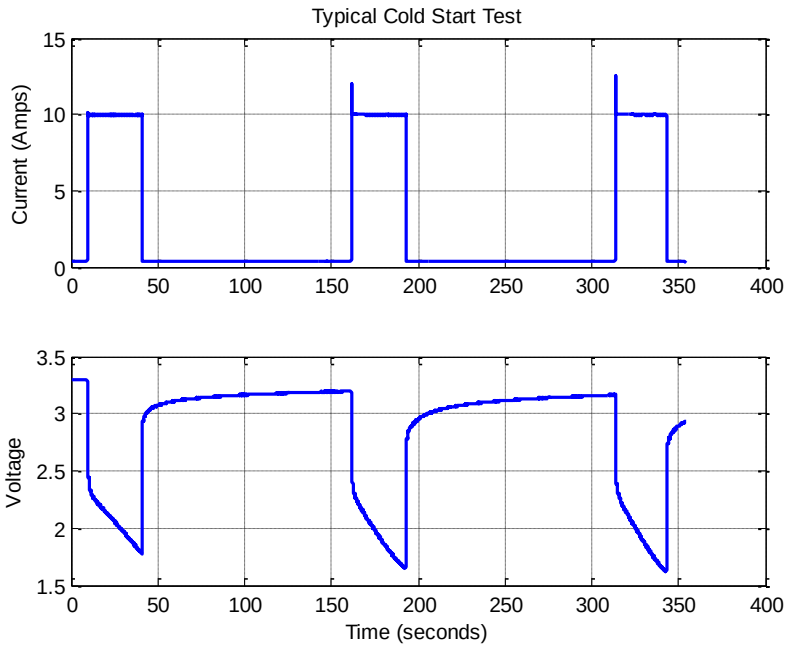

Figure 5: Typical Cold Start Test

The trial that was run most frequently was the aging cycle. This program consisted of a repeated square wave current pattern where the battery was charged and discharged by the same amount. The size and length of each charge / discharge block was determined by the depth of discharge (DoD) prescribed for each battery. Depth of discharge is the percentage of state of charge that is being removed, typically in a single cycle. In this experiment, aging programs ranged from 375-1000 aging cycles per day. An example of a portion of an aging program is shown below in Figure 6.

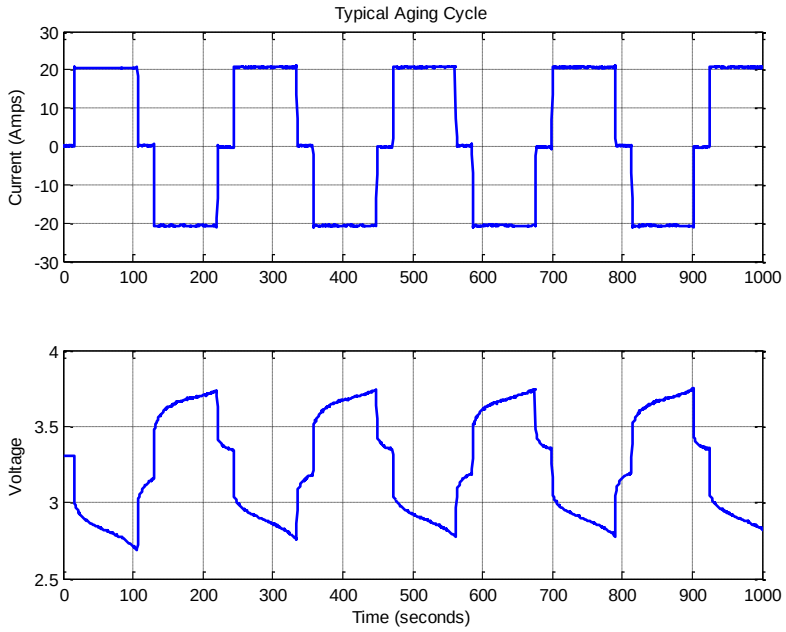

Figure 6: Typical Aging Cycle Profile

After each test was performed, no matter what type, the battery was reset to its prescribed SoC before another test was run. This was accomplished by fully charging the battery, and then removing a certain percentage of charge, calculated using the most recent capacity test. A typical SoC setting procedure is shown below in Figure 7

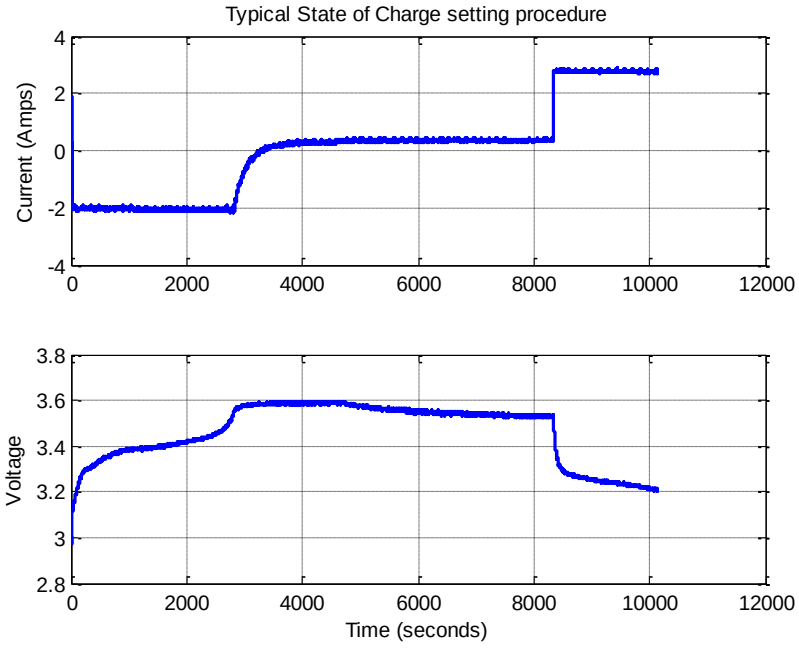

Figure 7: Typical State of Charge setting procedure

All of these tests were performed on A123 26650 2.3 amp hour cylindrical lithium-ion phosphate batteries, seen in Figure 8. In order to determine how severe one aging regimen is compared to others, aging cycles of different types were assigned to different batteries. Capacity, Pulse, and Cold start tests all remained the same, creation of different aging regimens was achieved by altering the aging cycles for each battery. This was accomplished by varying the SoC, DoD, and C-rate for different batteries. Before testing began, batteries were labeled "AXXX" where XXX was a three digit number identifying the battery. Batteries were then assigned a specific set of aging parameters that were maintained throughout the life of the battery. For a given battery, SoC was chosen as 70%, 50%, or 30%, DoD was 20% or 10%, and C-rate was either 8C or 16C. For this experiment, all batteries were held at a constant temperature of 45 °C. Table 1 summarizes how many batteries underwent each set of aging parameters that existed, and Table 2 lists the aging conditions for each battery. For the in depth analysis covered in chapter 3, battery A027 was chosen. This battery was held at 50% SoC and experienced 20% depth of discharge at a C-rate of 8C.

Figure 8: A123 Lithium-ion Phosphate battery

Table 1: Battery Aging Profile List

	70% SoC	50% SoC	30% SoC
10% Discharge 8C Rate	0	0	0
10% Discharge 16C Rate	2	2	4
20% Discharge 8C Rate	2	2	0
20% Discharge 16C Rate	4	2	0

Table 2: Catalog of Battery Aging Conditions

Battery	SoC	DoD	C-rate
A004	70	10	16
A005	50	10	16
A006	30	10	16
A007	30	10	16
A008	30	10	16
A009	50	10	16
A010	70	10	16
A011	30	10	16
A012	70	20	16
A014	50	20	16
A015	50	20	16
A016	70	20	16
A017	70	20	16
A018	50	20	16
A019	50	20	8
A027	50	20	8
A028	70	20	8
A029	70	20	8
A036	70	20	16

2.2 Data Modeling / Processing

In order to determine how a battery's life is affected by different aging scenarios, a method for determining what phase of life, or state of health (SoH), a battery is currently in was needed. To analytically determine this state of health, an appropriate model was used to represent the battery. Many types of battery models exist, including electrochemical models, fractional discharge battery models, dynamic lumped parameter battery models, equivalent circuit models, as well as hydrodynamic, and finite element models. Hu et al. [6] note that the Randle equivalent circuit model is often selected because of its simplicity and universality. For these reasons, the Randle model was chosen for use in this project.

Once the Randle equivalent circuit was selected as an adequate model, the order of the model needed to be decided. As mentioned earlier, the Randle equivalent circuit had any number of resistor / capacitor pairs, the number of these pairs determined the order of the model. The model order also defined how many parameters would need to be identified to determine the battery state of health. While higher order models were more capable of reproducing battery response, 2^{nd} order was the highest order considered in this project for the sake of simplicity.

2.2.1 Modeling

In this experiment, zeroeth order, first order, and second order Randle equivalent circuit models were considered. Each of these models had advantages and disadvantages that needed to be considered. The lower the model order, the less parameters that needed to be identified. However, as model order decreased, the model's voltage response became less and less representative of a real battery. These characteristics need to be balanced, and here the pros and cons of the three orders of models that were considered are described in detail.

2.2.1.1 Zeroeth Order Model

The zeroeth order equivalent circuit model was the simplest model and consisted of only two elements, an ideal voltage source and a resistor as seen in Figure 9. The resistor in this model represented the internal resistance of the battery, R_0, and the voltage source represented the open circuit voltage E_0. Although equivalent circuit models appear trivial, they are actually much more complicated due to the complexity of the parameters they contain. This simple model contained only two parameters to identify, however, the parameters in equivalent circuit models are not constant values. In this case, E_0 and R_0 are both functions are SoC, temperature, current direction (charge or discharge), and age. We can simplify these parameters in this project because all experiments occurred at constant temperature. Further simplifications were made for E_0 and R_0 as well. Open circuit voltage was assumed to depend only on SoC, and only current direction was considered for internal resistance because the small depth of discharge seen in this

experiment was not believed to contribute significant variations in resistance due to state of charge.

Although this model was simple to identify, it would have provided an extremely poor representation of actual battery voltage response. From equation 1 we can see this model failed to capture the dynamics that are present in battery response. The response of this zeroeth order model would appear as a square wave pattern centered around E_0, with amplitude equal to IR_0. For these reasons, the zeroeth order model was not chosen to simulate battery behavior.

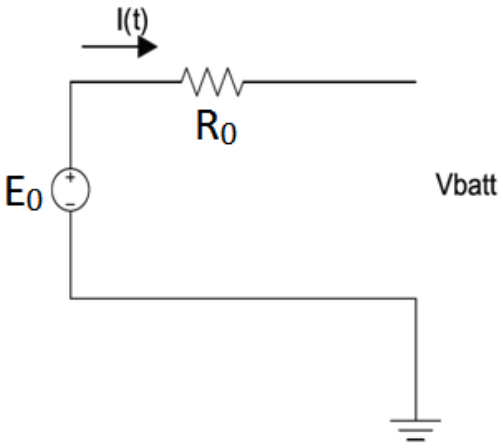

Figure 9: Zeroeth order Equivalent Circuit Model

$$V = E_0 - IR_0 \tag{1}$$

$$E_0 = f(SoC, T) \tag{2}$$

$$R_0 = f(SoC, T, \text{sign}(I)) \tag{3}$$

2.2.1.2 First order Model

The first order battery model was a much closer approximation than the zeroeth order model to true battery voltage response. As we can see from Figure 10, the first order model contained one resistor / capacitor pair in addition to the elements contained in the zeroeth order model. This resistor capacitor pair added two extra parameters to the system, a resistance and a capacitance, and resulted in a much better representation of true battery voltage response. The added resistance and capacitance were both dependent on current direction, SoC, and temperature, but the same assumptions made for internal resistance before were applied to both parameters.

The added resistor /capacitor pair was responsible for adding first order dynamics to the system, described by equations 4 and 5. This first order system was a much closer approximation of true battery behavior, but required more computational power than a simple zeroeth order model. Instead of identifying 3 parameters as in a zeroeth order system (E_0,R_{0c}, and R_{0d}), we are now required to identify seven; E_0, R_{0c}, R_{0d}, R_{1c}, R_{1d}, C_{1c}, C_{1d}, where c and d represent charge and discharge respectively..

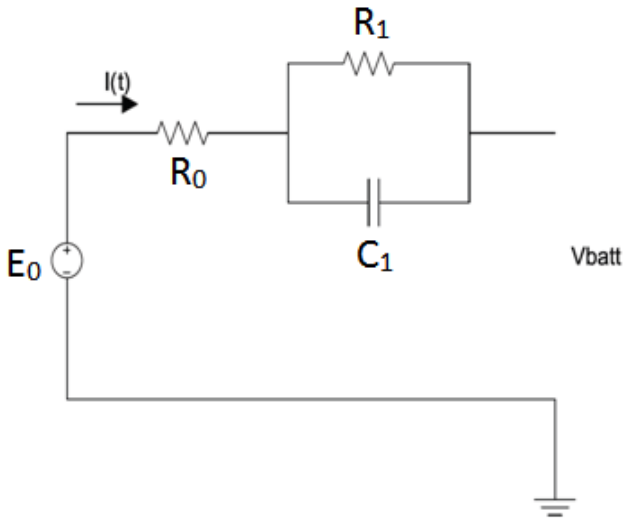

Figure 10: First Order Equivalent Circuit Model

$$V = E_0 - R_0 I - V_{C1} \tag{4}$$

$$\frac{dV_{C1}}{dt} + \frac{1}{R_1 C_1} V_{C1} = \frac{1}{C_1} \tag{5}$$

$$E_0 = f(SoC, T) \tag{6}$$

$$R_0, R_1, C_1 = f(SoC, T, \text{sign}(I)) \tag{7}$$

$$\alpha_1 = \frac{1}{R_1 C_1} \tag{8}$$

2.2.1.3 Second Order Model

The second order model was very similar to the first order in appearance, the only difference was an additional resistor / capacitor pair as seen in Figure 11. These additional components added four extra parameters to the battery model, a charge and discharge value for the second resistor and capacitor, bringing the total number of parameters that needed to be identified up to eleven. At this point, model identification required significant computing time and power, making this model of little use in a real time application like that of vehicle diagnostics. However, these added parameters did increase the accuracy of the second order model, as seen in Figure 12. The addition of the second resistor capacitor pair stacked a second, first order dynamic system, on top of the one obtained in the first order model. To clarify, the second order model did not introduce second order dynamics, it merely summed the effects of two sets of first order dynamics as seen in equations 9, 10, and 11, allowing the model to represent a wider range of battery responses. It was because of this increased versatility that a second order model was chosen for use in simulating battery voltage and identifying battery parameters.

$$V = E_0 - R_0 I - V_{C1} - V_{C2} \tag{9}$$

$$\frac{dV_{C1}}{dt} + \frac{1}{R_1 C_1} V_{C1} = \frac{1}{C_1} \tag{10}$$

$$\frac{dV_{C2}}{dt} + \frac{1}{R_2 C_2} V_{C2} = \frac{1}{C_2} \tag{11}$$

$$E_0 = f(SoC, T) \tag{12}$$

$$R_0, R_1, R_2, C_1, C_2 = f(SoC, T, \text{sign}(I)) \tag{13}$$

$$\alpha_1 = \frac{1}{R_1 C_1} \tag{14}$$

$$\alpha_2 = \frac{1}{R_2 C_2} \tag{15}$$

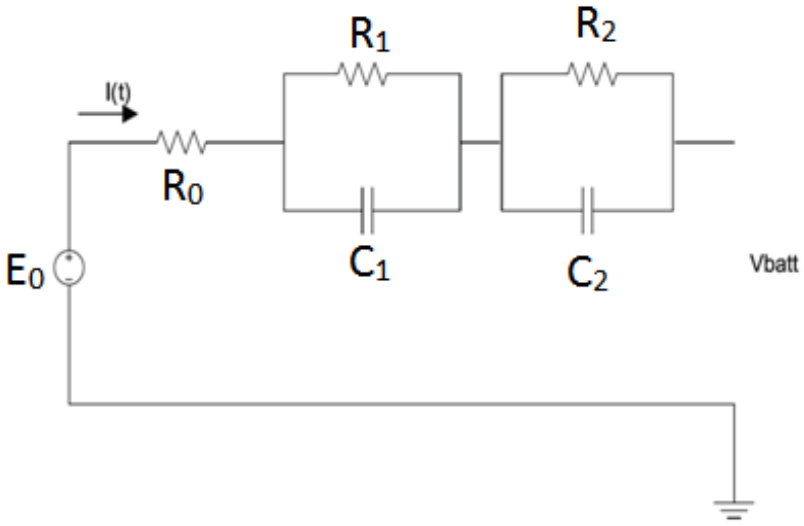

Figure 11: Second Order Equivalent Circuit Model

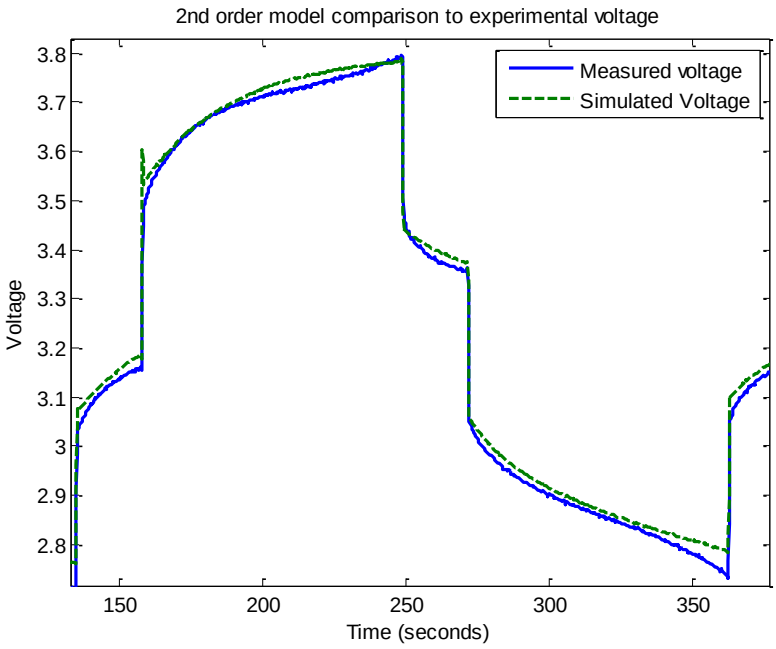

Figure 12: Sample Second Order Simulation Results

2.2.2 Data pre-processing

When simulating battery voltage and identifying battery parameters, certain steps were taken to pre-process the experimental data in order to make these tasks simpler and more accurate. When the experimental data was collected, a large amount of noise was present in the current and voltage signals as seen in Figure 13. Since the current signal was used as an input to the Simulink model, and the voltage signal was used to calculate the error between the experimental and simulated voltages, this noise would have resulted in larger errors when performing battery simulation and identification. To combat these issues, averaging techniques were used to remove the noise from both signals.

Data was segmented so that one day of aging cycles was contained in a single file. This meant that in a single aging file there were anywhere from 300 to 1000 charge and discharge cycles. Matlab was used to identify and isolate the current and voltage data for every aging cycle in a single data file. The length of each aging cycle was then computed because aging cycle length could vary by up to a second. Once cycle length had been calculated, the most commonly occurring cycle length was determined and all voltage and current cycles of this length were averaged together to create a single voltage and current cycle. Due to the fact that the noise present in the data was random, the averaging of hundreds of aging cycles caused most of the noise to cancel itself out, and the result was a clean, or ideal, current or voltage pattern. These ideal current and voltage patterns were then repeated ten times to create an signal long enough to input into the simulator, and compare the generated voltage against, as seen in Figure 14.

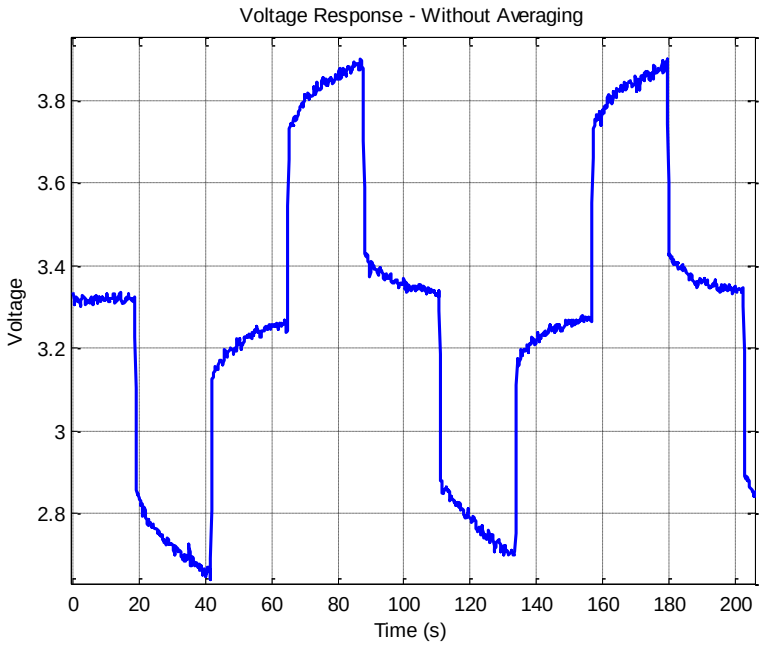

Figure 13: Unprocessed Voltage Pattern (noisy)

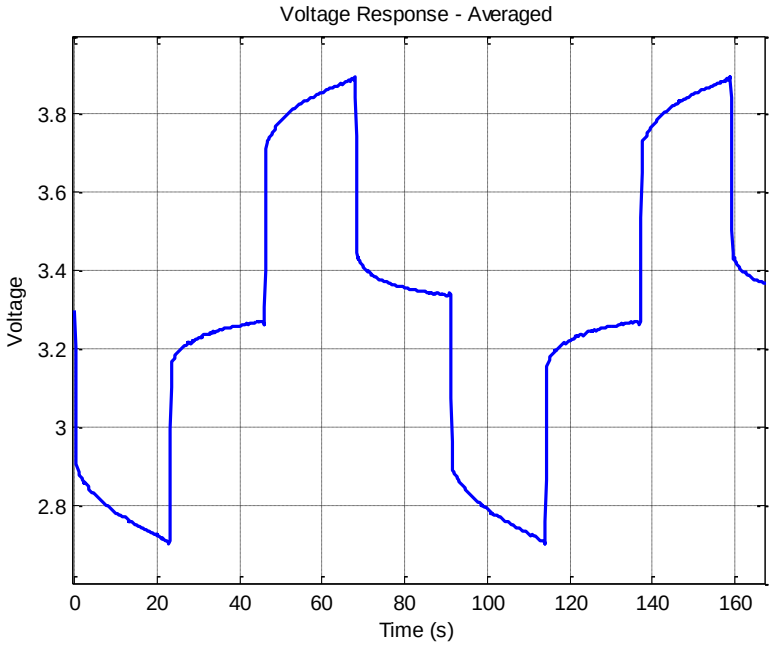

Figure 14: Processed Voltage Pattern (clean)

2.2.3 Model Identification

The model and its governing equations were implemented using Matlab and Simulink. The use of these software tools allowed automated identification of the battery to be performed. Parameters were optimized by minimizing the error between the simulated voltage response and experimental response. The parameters that achieved this goal were assumed to be an accurate representation of the battery at a current state of health. Once parameters were identified at a given point in time, they were recorded and the process was repeated for all aging files over the life of a battery.

As mentioned, Simulink was utilized to implement the battery model in this project. This required a number of battery subsystems to be modeled in the Simulink environment. To accurately capture the behavior of a battery, the differential equations describing the battery behavior needed to be modeled, the open circuit voltage of the battery needed to be modeled using methods explored by Hu et al., and the model parameters needed to be scheduled based on whether the battery was charging or discharging.

Initially, only the differential equations needed to describe the battery were programmed using Simulink. These initial models provided a relatively close fit to the voltage of an actual battery but they were only capable of capturing the rough shape of the voltage response, not the subtle nuances that appeared in batteries' responses as they aged. In order to create a closer match to the true voltage response of a battery, the behavior of the open circuit voltage needed to be modeled.

The open circuit voltage subsystem was created in order to allow the simulated voltage response to more closely recreate the response of an actual battery. Particularly as batteries aged, they began to display exaggerated peaks and valleys at the top and bottom of each aging cycle as displayed in Figure 15. This was eventually discovered to be caused by the open circuit voltage behavior of the battery. Using equation 9 where z is battery state of charge, developed by Hu et al. the battery open circuit voltage behavior was programmed as a subsystem into the Simulink model. The coefficients in this equation were optimized using matlab. Each time a new aging file was being analyzed, the capacity test closest to the current aging file was located. The open circuit voltage curves created in this capacity test were then averaged together and curve fitted as seen in Figure 16, yielding the coefficients needed in the equation 16.

$$E_{OC}(z) = V_0 + \alpha(1-\exp(-\beta z)) + \gamma z + \zeta(1-\exp\left(-\frac{\varepsilon}{1-z}\right)) \tag{16}$$

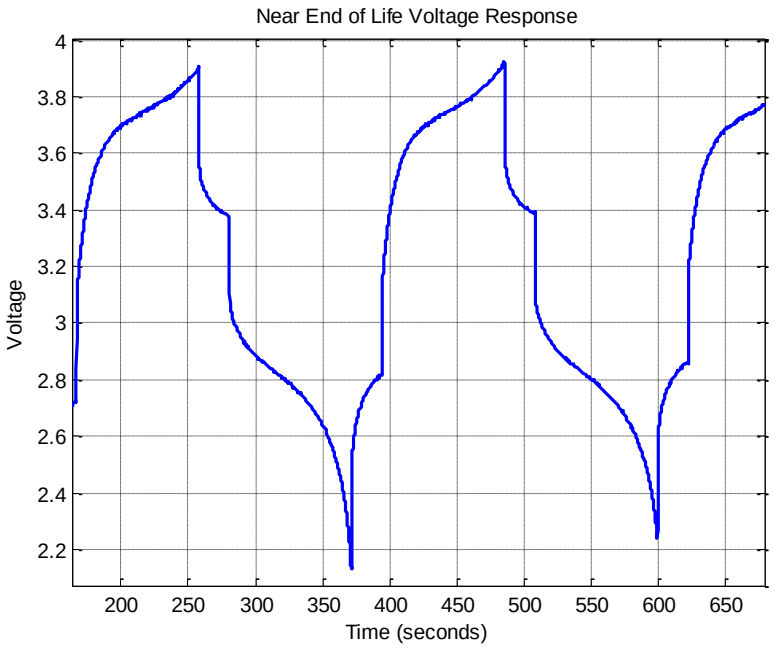

Figure 15: End of Life Voltage Response

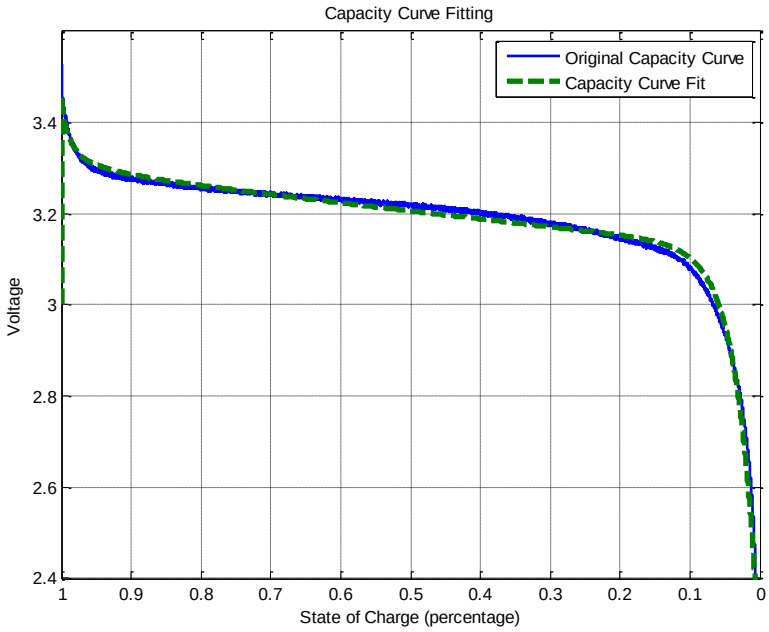

Figure 16: Open Circuit Voltage Curve Fitting

Battery parameters are not constant values, they are functions of temperature, state of charge, and current direction. In this experiment, temperature was constant and state of charge was held in a limited range so these parameter dependencies were ignored. This meant that at a given state of health, battery parameters depended on current direction. This is the reason separate parameters needed to be modeled and identified for when the battery was being charged and discharged. The last subsystem that needed to be included in the Simulink model was a method for scheduling parameters based on the direction of current. This was accomplished by creating two banks of parameters, one to represent both charging and discharging situations. The appropriate parameters were fed into the model based on whether the battery was charging or discharging based on the sign of the current. When current was positive, discharging parameters were used, and the opposite for when current was negative.

Using these methods, a suitable battery model was implemented using Matlab and Simulink. The input to the model was a set of battery parameters and the ideal current pattern created during the data pre-processing procedure, the output of the model was a simulated voltage pattern. Depending on the parameters input into the model, this simulated voltage may be drastically different from experimental voltage obtained in the lab as seen in Figure 17. The last step in using the battery simulator to identify battery parameters was to find the set of parameters that minimized the error between the simulated voltage and the experimental voltage obtained in the battery aging lab.

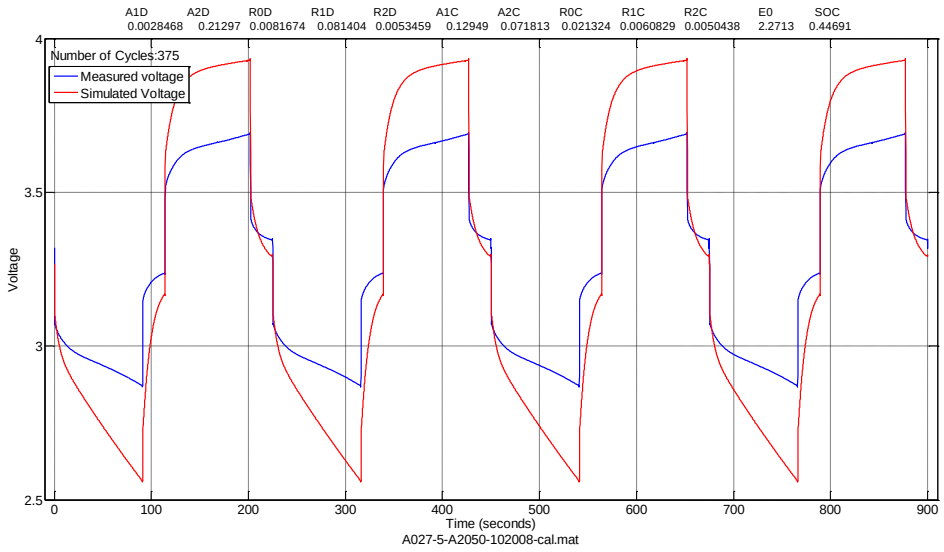

Figure 17: Voltage Response Comparison with Guessed Parameters

Matlab was used to minimize the error between simulated and experimental voltage response. A matlab function was written that received a set of parameters, simulated battery response, and calculated the error corresponding to this response. This function was then used in conjunction with the matlab optimization function fgoalattain. Fgoalattain allowed us to set multiple goals that needed to be achieved, as well as how much weight should be placed on reaching each goal. The two goals in this case were for the average value of the error and the standard deviation of the error to both equal zero, and they were both given equal weight.

Initially, error was quite large as seen in Figure 18. Starting from this incorrect initial guess of battery parameters, fgoalattain ran thousands of iterations, varying battery parameters each time, in order to find the combination of parameters that resulted in the smallest error based on the defined goals. Once the error was minimized as seen in Figure 19, the parameters that achieved this error were recorded and more aging analyses were run.

To expedite the process of performing this analysis on every aging file that was available, Matlab was used to automate the process. A matlab script was written that allowed the user to select which battery was to be analyzed. Matlab then performed the optimization process and recorded the results for every aging file available for that battery. To make results more accurate, the optimized parameters for one day of aging were used as the initial guess for the next day of aging. Once all available aging data was analyzed, the resulting parameters were inspected for trends.

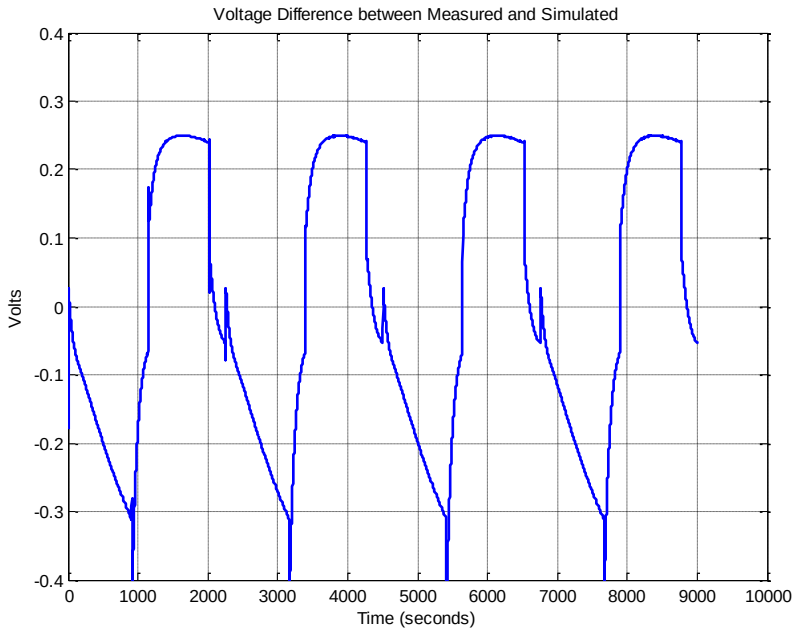

Figure 18: Large Error Resulting from Incorrect Battery Parameters

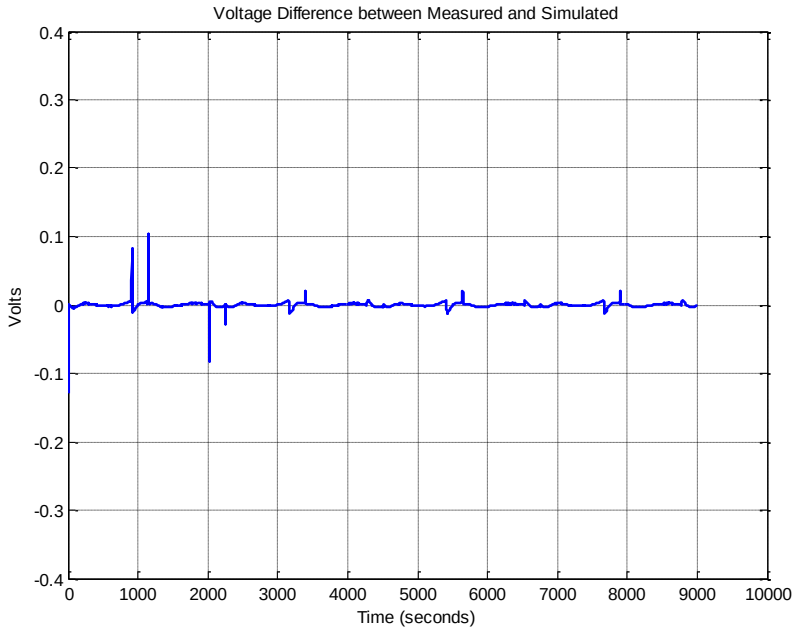

Figure 19: Small Error Resulting from Correct Battery Parameters

2.2.4 Method for Estimating Internal Resistance

Besides battery simulation and parameter identification, there was another method that was utilized in this project to identify trends in battery aging. This second method utilized a zeroeth order model to provide information regarding the rate at which batteries aged. As we have already seen, the voltage response of a battery required two first order dynamic systems to be accurately represented so it was obvious that a zeroeth order model could not capture this aspect of battery behavior. However, if the dynamic response of the battery is ignored then a zeroeth order model could be used to obtain information from the abrupt voltage changes seen in this experiment, shown in Figure 20.

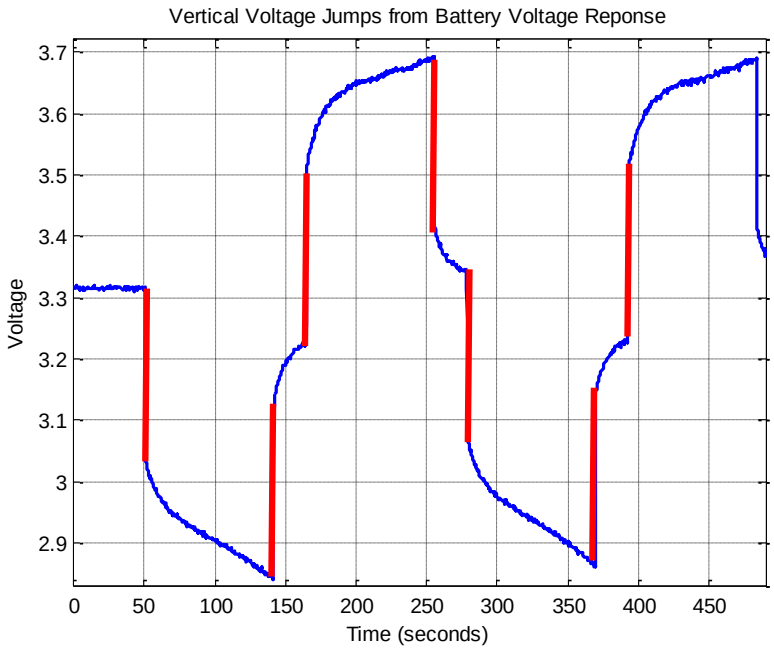

Figure 20: Vertical Jumps Seen in Battery Voltage Response

This method for estimating internal resistance used the governing equation of the zeroeth order model to calculate a value of internal resistance each time current is applied or removed. This was accomplished by isolating each vertical voltage jump and considering only the change in voltage that occurs, not the absolute values of voltage. If these voltage jumps were isolated, equation 1 which was used to describe the zeroeth order model became equation 17, which is essentially Ohm's Law. By measuring the voltage difference that occurred at each voltage jump, and dividing by the known amount of current that was applied or removed, we obtained a value of internal resistance, R.

$$\Delta V = \Delta I \bullet R \tag{17}$$

In this case, the calculation of internal resistance was trivial and could be performed quickly for each aging file. For each aging cycle, current was applied and removed a total of four times, which resulted in four values of internal resistance for every aging cycle. Typically, batteries underwent 10,000 or more aging cycles, which resulted in a very large number of resistance values for each battery as seen in the sample analysis displayed in Figure 21.

This Figure also illustrates the large amount of noise that was present in this measurement. To remove the noise from these resistance values, an averaging procedure similar to the one used to pre-process data was used. All four sets of resistance values were averaged together to create a single set of resistance values as seen in Figure 22. Then every 100 resistance values were averaged together, resulting in the reduced data set displayed in Figure 23.

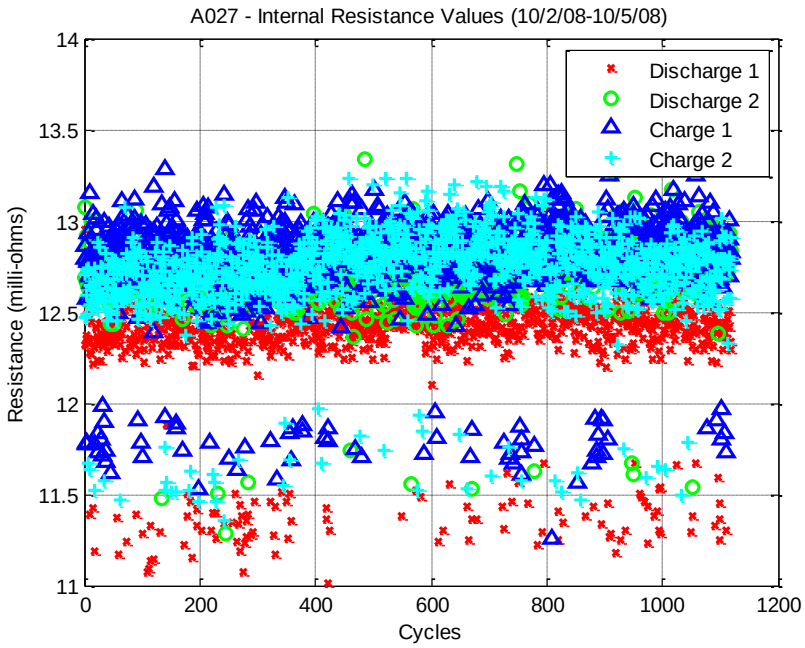

Figure 21: Values Obtained from Internal Resistance Estimation Method

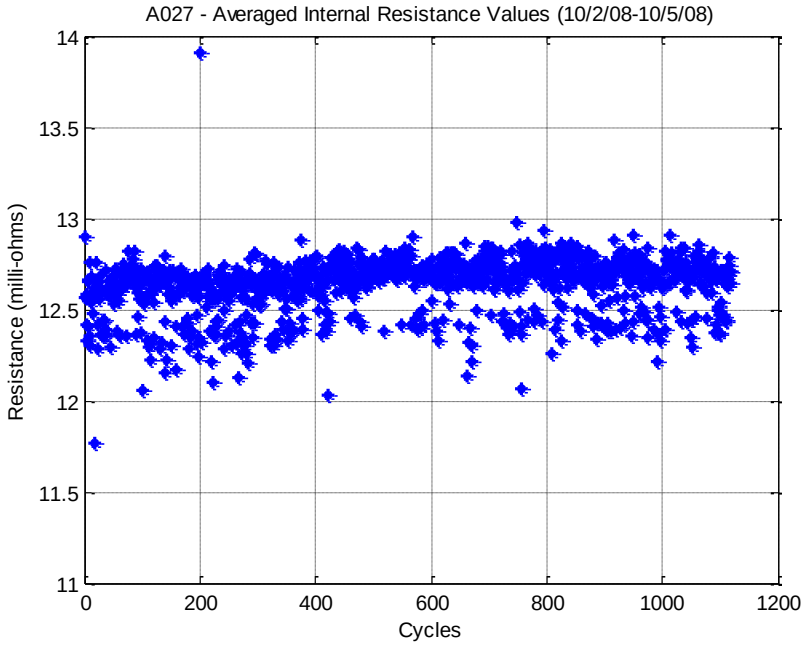

Figure 22: Averaged Values from Internal Resistance Estimation Method

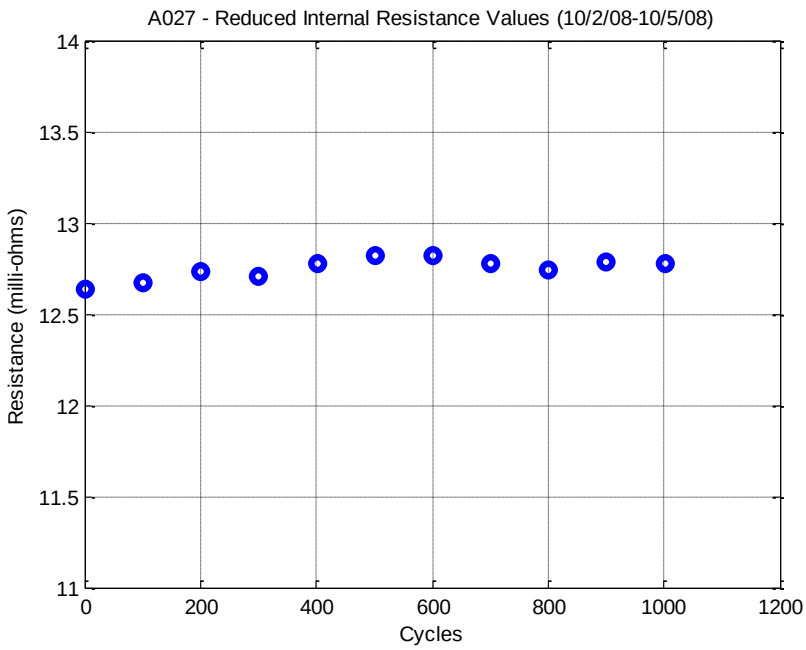

Figure 23: Reduced Values Obtained from Internal Resistance Estimation Method

After this analysis was carried out for the entire catalog of aging data for a single battery, the next step was to curve fit the data as displayed in. By curve fitting the data, we were able to attach a numerical value to the growth of the internal resistance. This numerical value could potentially be related back to the conditions under which a battery was aged, lending insight to how different aging conditions affect the rate at which a battery ages. It is also worth noting that this large amount of internal resistance data was collected very easily, and at very little computational cost. If suitable trends are visible in internal resistance growth over time, they could be correlated to battery state of health. This method could become a very cheap and useful way to estimate battery life.

CHAPTER 3

DETAILED RESULT IN ONE BATTERY

After explaining how batteries were systematically aged in this experiment and the methodology behind the analysis of this aging, we now turn to the results of this analysis. This chapter will highlight the results achieved from the in depth analysis of a single lithium ion battery, with broader trends discussed in the following chapter. Battery A027 was chosen as the candidate for in depth analysis. As mentioned, this battery was chosen because it contained one of the largest data sets, which allowed for a more comprehensive analysis. A027 was held at 50% state of charge and underwent a 20% depth of discharge at 45°C, as seen in Table 2. There were a total of 75 days of aging data and 17 capacity tests spaced throughout the life of the battery between October 2, 2008 and February 28, 2009. First the results of the parameter identification will be discussed, followed by trends identified in the growth of internal resistance seen in data collected from the internal resistance estimation technique.

3.1 Parameter (model) identification

Battery parameter identification was carried out extensively for battery A027. Rather than identify parameters for every day of aging data, every other aging file was analyzed. This choice was made in order to reduce computation time and is justified by the relatively small amount of change a battery experienced due to aging in this time frame. The simulator was capable of producing very accurate results, as seen in Figure 24. However, as batteries neared the end of life, the results produced by the simulator became less accurate, as seen in Figure 25.

This degradation of simulator accuracy was most likely caused by severe reduction in battery capacity. The large peaks and valleys seen in the end of life battery response were most likely attributed to the open circuit voltage curve of the battery. As capacity decreased, the voltage of the battery travelled along the open circuit voltage curve much more rapidly, apparently reaching low enough states of charge to pass the "elbow" of the open circuit voltage curve. Although this shortcoming of the model was significant, it was only observed in the final days of aging and should not be considered indicative of all results produced by the simulator.

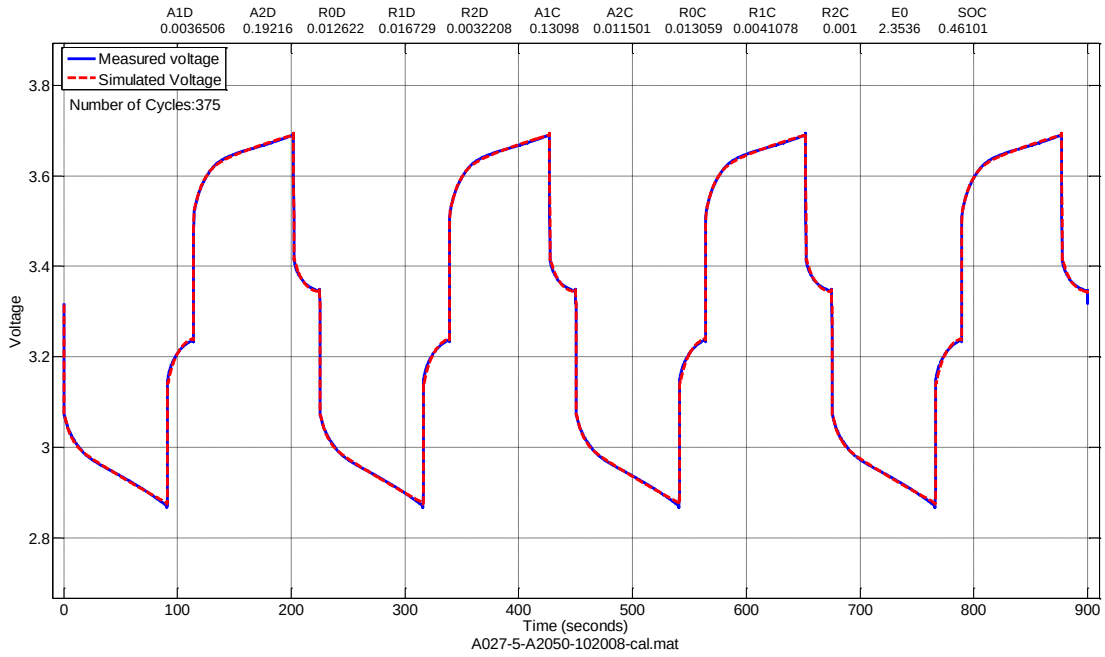

Figure 24: Second Order Simulation Results (A027 – 10/18/2008)

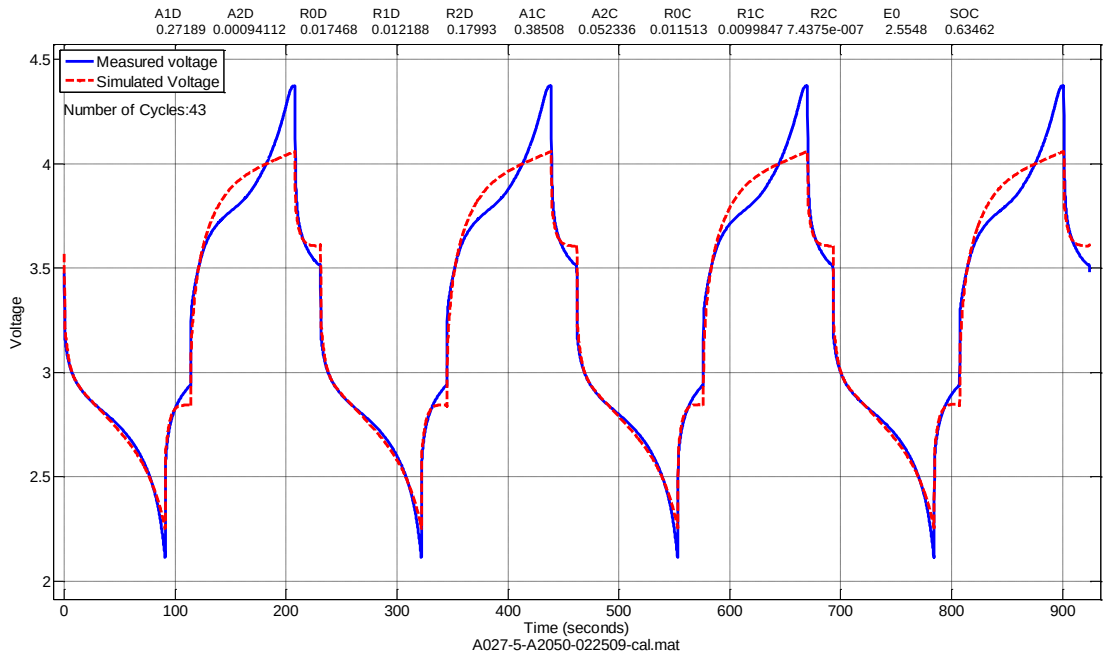

Figure 25: Second Order Simulation Results (A027 - 2/25/09)

As mentioned previously, approximately half of the 75 days of available aging data for battery A027 were analyzed, resulting in a set of 39 identified parameters. Rather than identify the value of the capacitors in the two resistor and capacitor pairs, 1/RC was identified instead. This expression was present in the differential equations describing battery voltage and will be referred to as α_1 or α_2. Ten battery parameters were defined at each identification, 2 values for α_1, α_2, R_0, R_1, and R_2, all parameters that were necessary to define a second order battery model.. The following pages display Figure 26 through Figure 30, comparisons of discharge and charge values for each parameter.

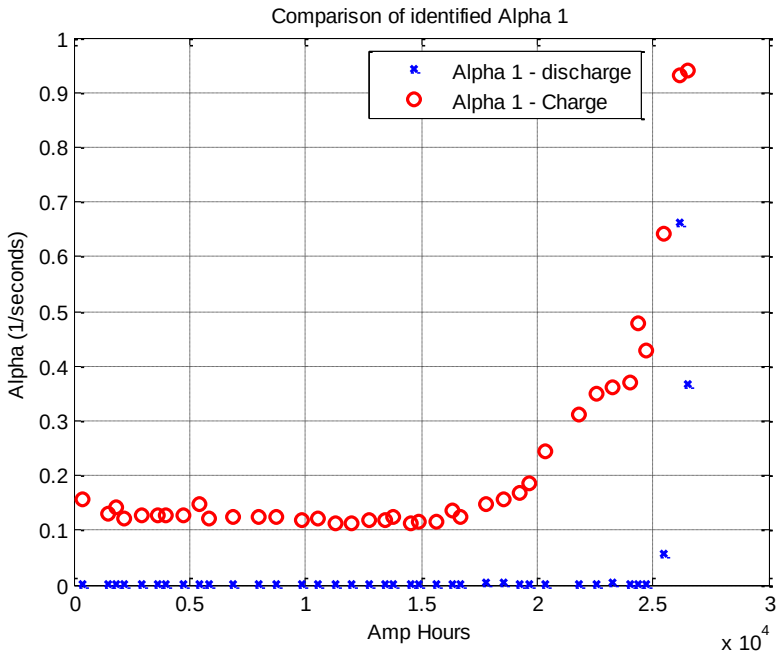

Figure 26: Comparison of Identified Parameter – α_1

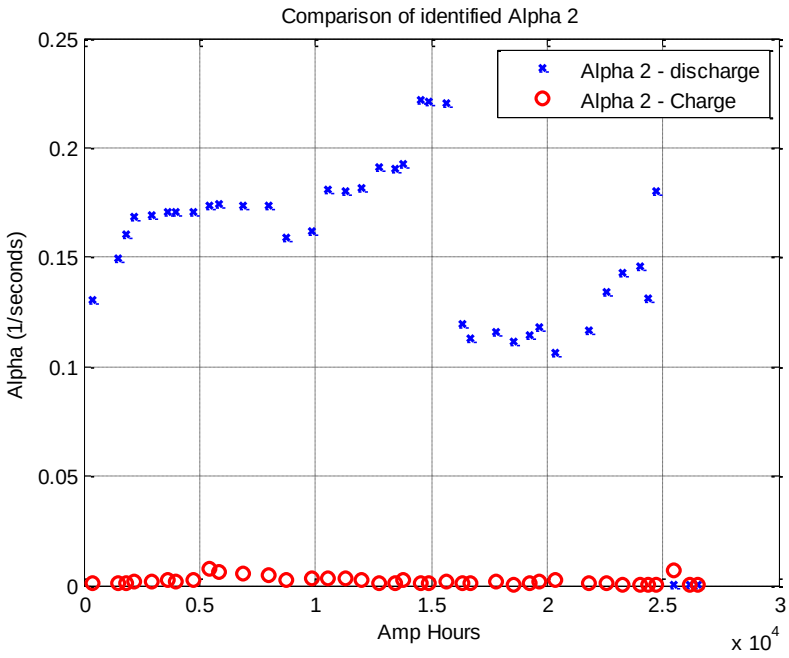

Figure 27: Comparison of Identified Parameter – α_2

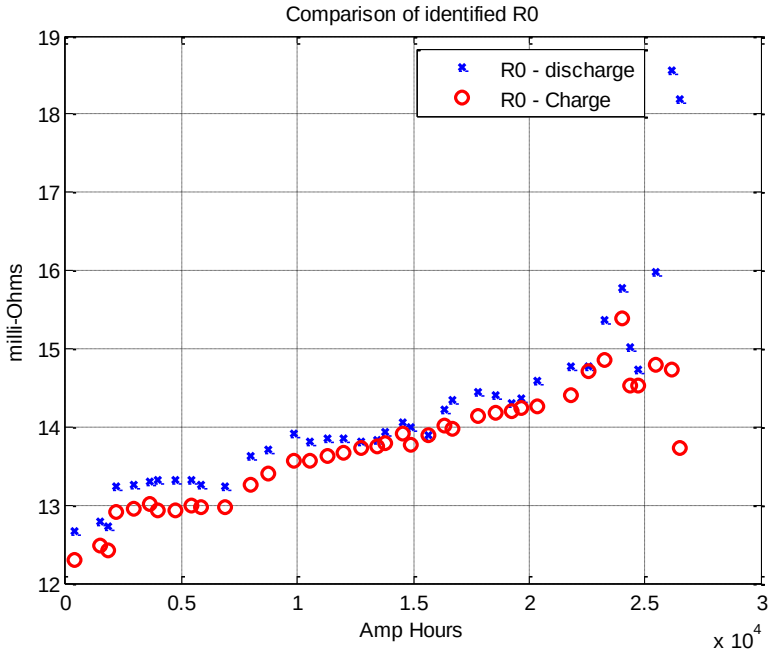

Figure 28: Comparison of Identified Parameter – R_0

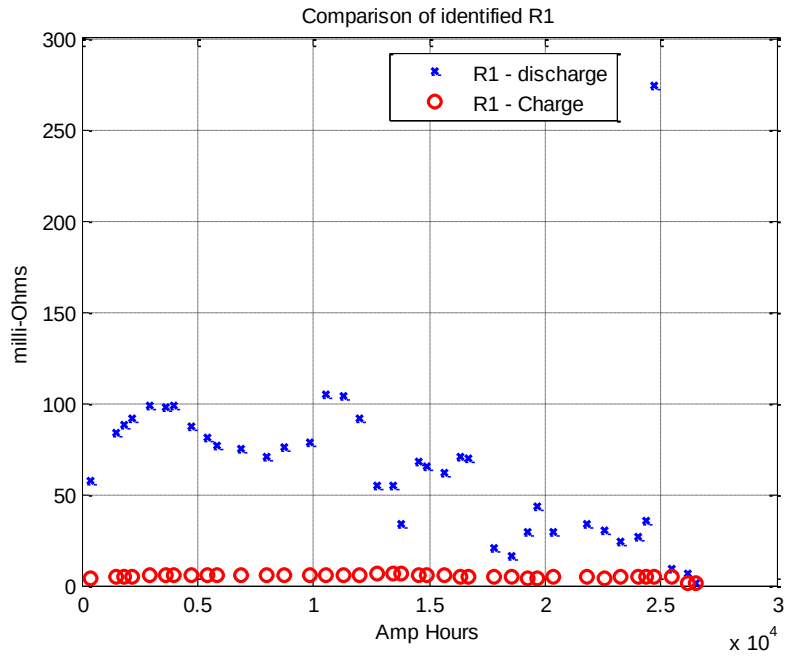

Figure 29: Comparison of Identified Parameter – R_1

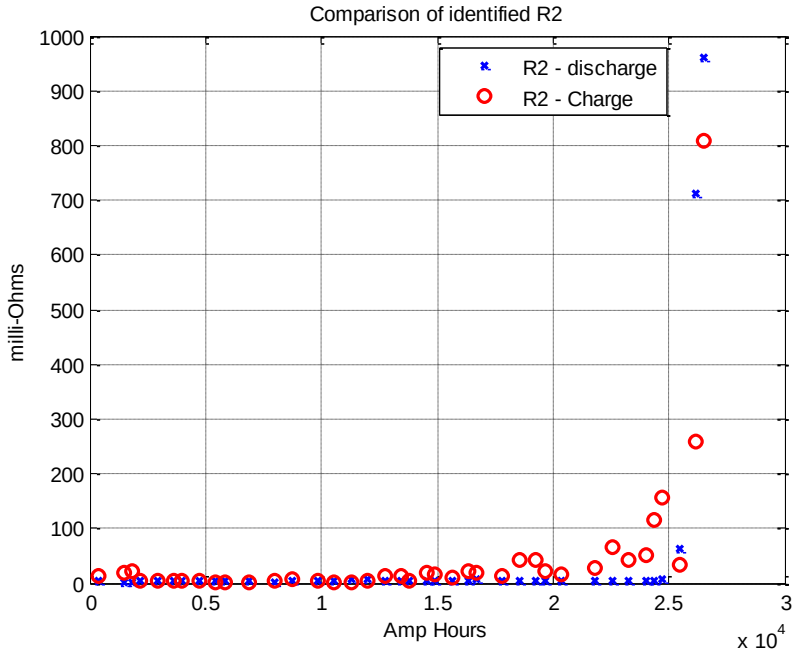

Figure 30: Comparison of Identified Parameter – R_2

The results of this analysis were far from consistent. One would expect charge and discharge values of the same parameter to be rather close, however for most of the parameters identified, this was not the case. Particularly, α_1, α_2, R_1, and R_2, all displayed this behavior. Although, while discharge and charge values for a single parameter such as α_1 did not match up, discharge values for one parameter and charge values of another were much closer. This was the case when comparing α_1 discharge and α_2 charge values. This was also true for the remaining α values, as well as values for R_1 and R_2. These new comparisons are displayed in Figure 31, Figure 32, Figure 34, and Figure 35, while Figure 33 repeats the same comparison for R_0 seen previously.

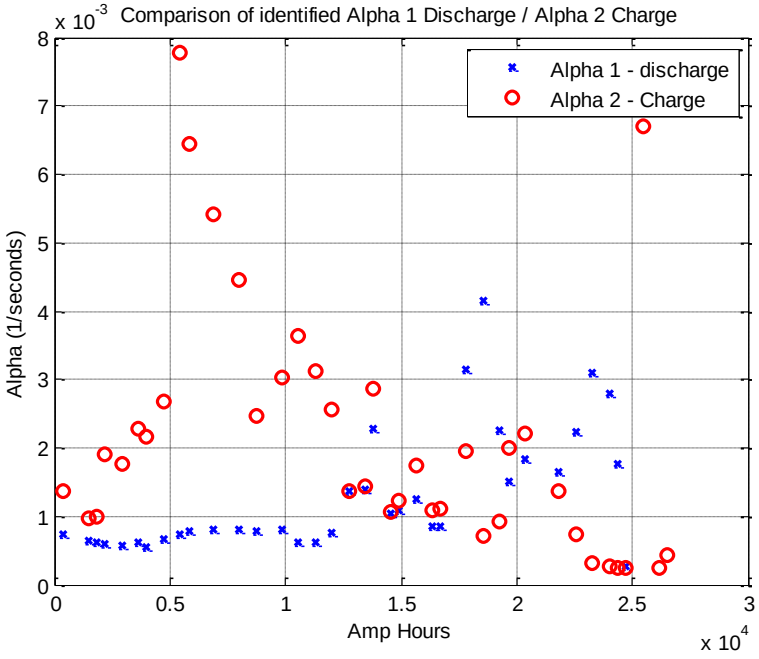

Figure 31: Combined Comparison of α_1 Discharge and α_2 Charge

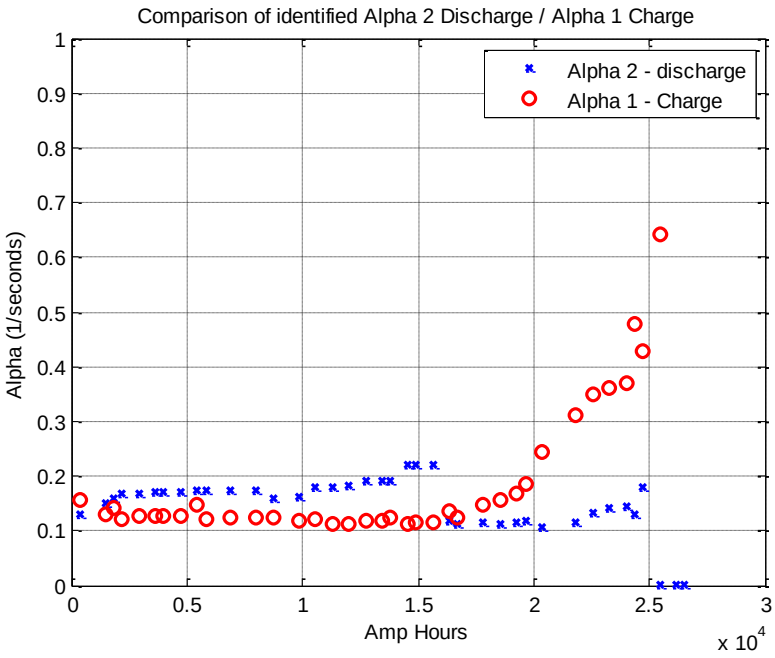

Figure 32: Combined Comparison of α_2 Discharge and α_1 Charge

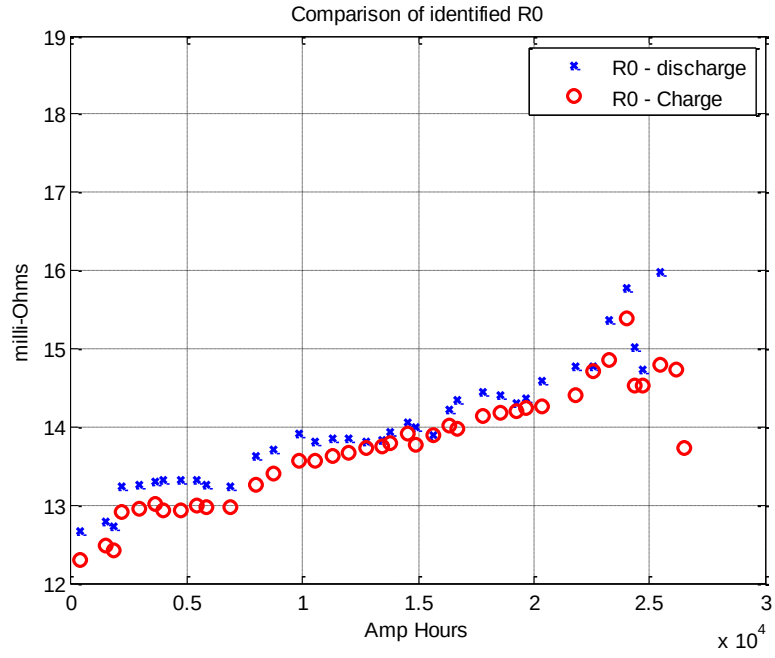

Figure 33: Comparison of Identified Parameter R_0

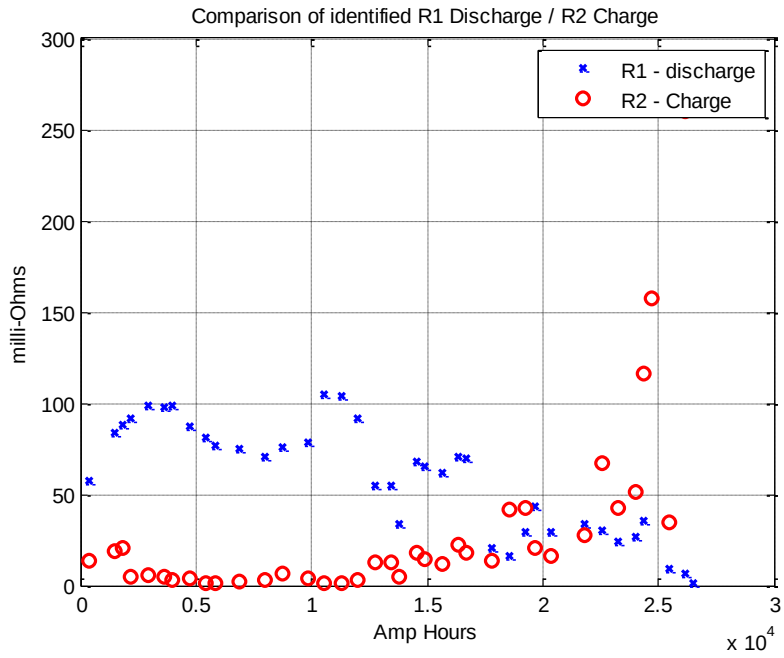

Figure 34: Combined Comparison of R_1 Discharge and R_2 Charge

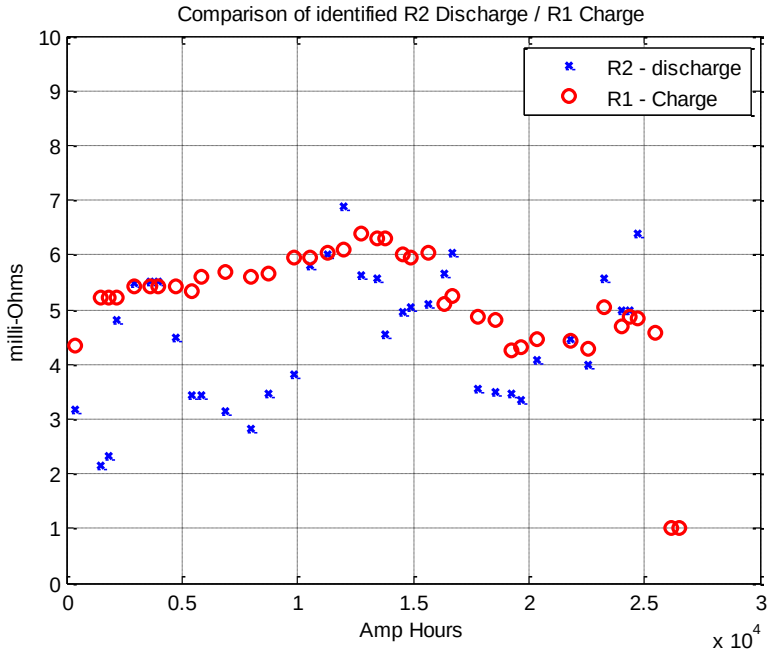

Figure 35: Combined Comparison of R_2 Discharge and R_1 Charge

When viewed in this manner, the results were much easier to compare. Beginning with Figure 31, the comparison of α_1 discharge and α_2 charge, these two parameters did not display any strong trends. α_1 discharge remained relatively consistent for much of the aging period and values eventually scattered halfway through the identification. The parameter α_2 discharge returned scattered values throughout most of the aging period. These scattered values seemed to indicate that the true aging behavior of the battery, a slow and consistent process, was not being captured by the identification.

Figure 32 displays the comparison of α_2 discharge and α_1 charge. These two parameters displayed much less scattering than the other α values. These consistent results seemed promising. However, at the end of the identification, α_2 discharge values decreased significantly and $\alpha_1$charge values increased sharply. If these parameters were truly indicative of the aging process inside the battery, we would expect them to trend together.

The comparison of charge and discharge values of R_0 can be seen in Figure 28 and Figure 33. This parameter displayed a very strong trend that was very nearly linearly increasing in value. The fact that both charge and discharge values of this parameter are very close and follow the same trend led to the conclusion that these results are an accurate representation of aging processes taking place within the battery.

Unfortunately, the comparison of values for R_1 discharge and R_2 charge was nowhere near as promising as that of R_0. The charge and discharge values seemed to follow opposing trends, with R_1 discharge trending towards zero at the end of life and R_2

charge values trending upward. Although these values exhibited values that developed slowly, with lower amounts of scatter, neither of these sets of values seem to accurately represent the process of battery aging.

The comparison of R_2 discharge and R_1 charge returned mixed results as well. Figure 35 displays this comparison, in which we see large amounts of scattered resistance values for R_2 discharge. Values obtained for R_1 charge moved much more slowly, but did not exhibit any trends consistent with battery aging.

Considering all of the trends observed in these comparisons, the strong linear increase observed in R_0 was by far the most informative. While some of the data showed trends on individual bases, none of the other trends were consistent within a single parameter. The cause for this is most likely the method used to obtain these parameters. In minimizing the error, Matlab sought only parameters that satisfied this criterion. Optimization functions used in this experiment did not search for parameters with the intention of maintaining trends in parameter growth, they identified parameters in a blind search based only on minimizing error. This fact, coupled with an initial guess that was not necessarily representative of true battery parameters, led to the overall failure of the simulator to provide meaningful trends observed in battery aging parameters.

Since the only meaningful result obtained from this analysis was the trend seen in R_0 growth, it was decided to focus on the method of analysis developed specifically for measuring internal resistance which was much more effective in this regard. The remainder of the results discussed in this report were obtained through this method.

3.2 Internal Resistance Estimation

The method for internal resistance estimation used in this project utilized the fundamentals of the zeroeth order battery model to calculate the internal resistance of a battery. This calculation was performed every time current was applied or removed, resulting in a very large number of internal resistance values. The analysis described in section 2.2.4. was initially performed on all aging files of the battery A027, which yielded the resistance measurements seen in Figure 36.

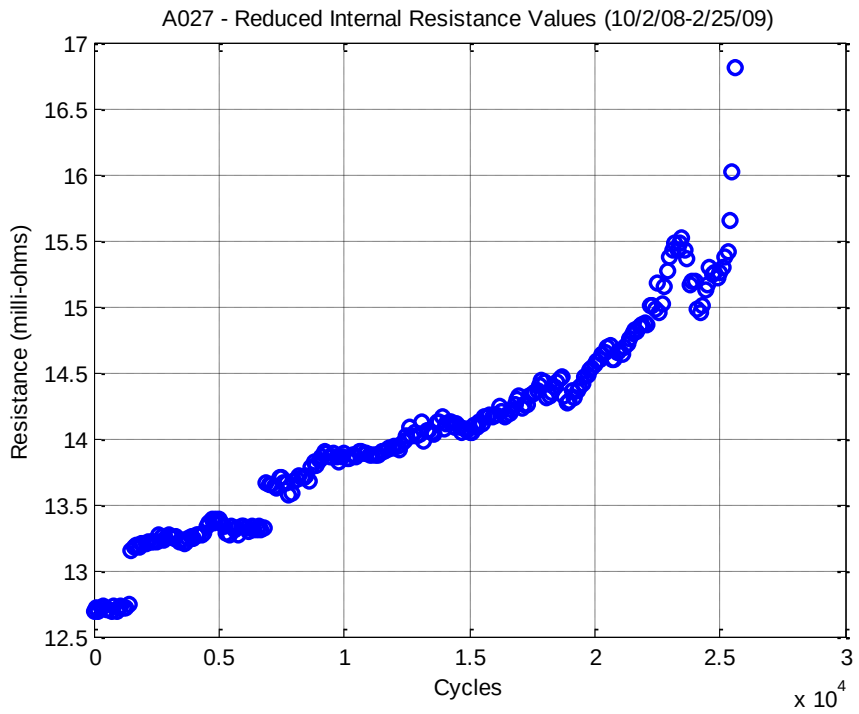

Figure 36: Internal Resistance Values of Battery A027

This Figure displays all resistance measurements plotted with respect to how many aging cycles the battery had undergone at the time each measurement was taken. This result verifies the trend observed when identifying battery parameters with a second order model as a near linear trend is observed for the large majority of life, followed by a sharp spike in resistance at the end of battery life.

For batteries, increased internal resistance had a number of implications. On a physical level, increased internal resistance indicated a physical degradation of a battery's innards. This degradation caused losses of speed and efficiency in the electrochemical reactions taking place in the battery. Increased internal resistance also had a large effect on the performance of a battery, the most notable of these effects was a loss of battery power. As internal resistance increased, the voltage drop due to an applied current became larger. Because power is proportional to voltage, this resulted in a loss of rated power for a battery.

A clear trend in the growth of internal resistance was identified in a single battery using two independent methods. Next, the more efficient method of estimating internal resistance was applied to a multitude of battery aging scenarios.

CHAPTER 4

EVOLUTION OF INTERNAL RESISTANCE WITH AGING

After the methods for estimating internal resistance were fine tuned for a single battery, this analysis was carried out on all batteries for which sufficient aging data existed. The purpose of carrying out this analysis on a number of batteries aged under a range of conditions was to determine whether or not the conditions under which a battery are aged have a significant effect on the rate at which this aging occurs.

In order to compare the rates at which different batteries aged in terms of internal resistance, care was taken to ensure consistency of units across all batteries. Up to this point, the standard measurement of age was a cycle. However, when dealing with different aging scenarios not every cycle was equivalent. To solve this issue, the x axis unit was changed from cycles, to amp hours. This was done by calculating the number of amp hours (a unit of electrical charge) that existed in a single cycle for each aging scenario. Simply multiplying the number of cycles by this scalar value accomplished the conversion.

The same approach was taken with respect to values of internal resistance. Not every battery began life at the same value of internal resistance, nor did every battery

experience the same numerical amount of internal resistance growth. In order to compare the internal resistance growth of multiple batteries, internal resistance values were converted to reflect the percentage increase a battery experience from its initial internal resistance value. This was easily accomplished by dividing all internal resistance values for a single battery by the initial internal resistance of that battery.

After the units for all sets of internal resistance data were made consistent, a comparison could be made between all sets of data. This comparison is shown in Figure 37, with a detailed view of curves closer to the origin displayed in Figure 38.

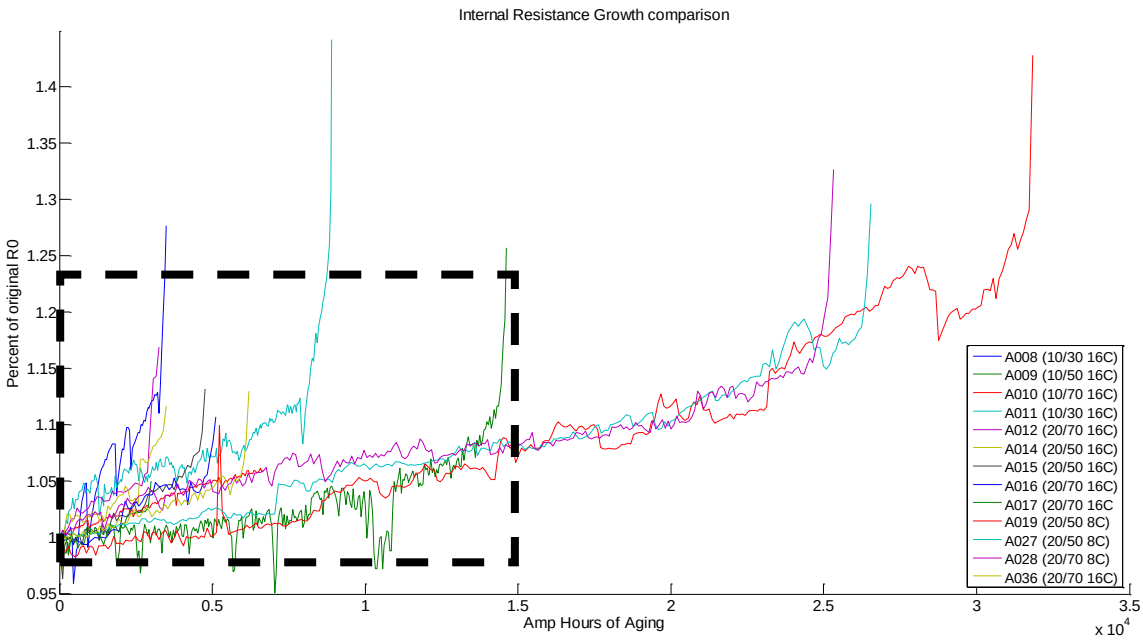

Figure 37: Comparison of Internal Resistance Growth for All Aging Scenarios

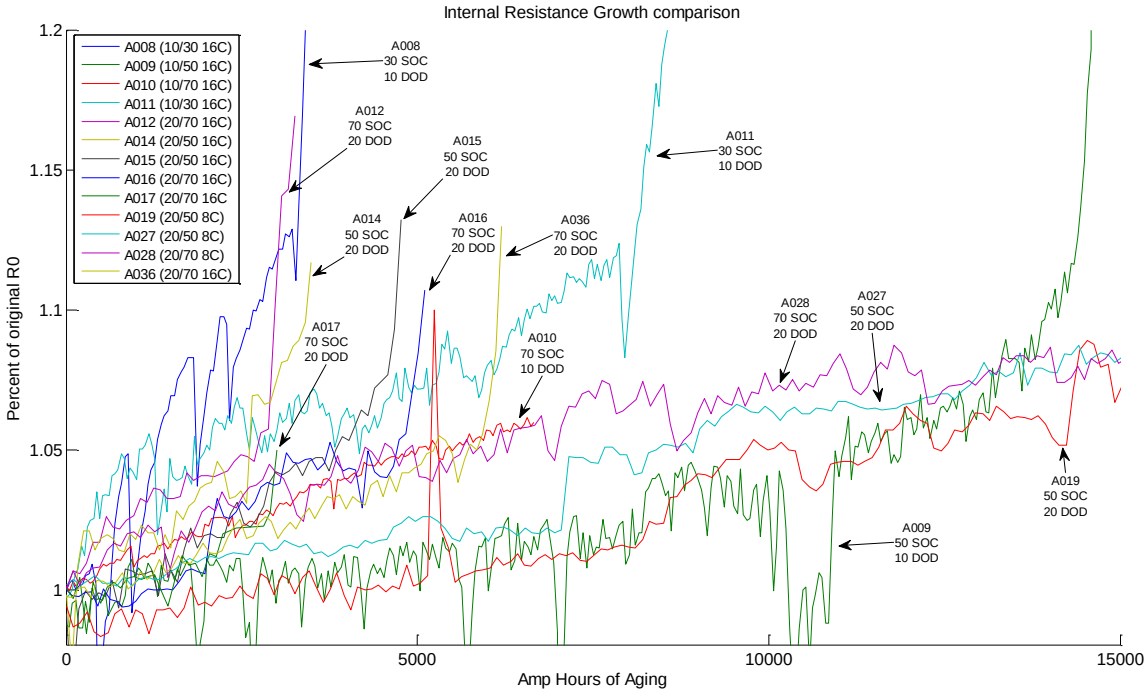

Figure 38: Detail Comparison of Internal Resistance Growth for All Aging Scenarios

Viewing the comparison of internal resistance growth curves, we see that all curves generally followed the same trend but slope differed greatly across the wide range of aging scenarios. This observation confirmed that the conditions under which a battery are aged have a large effect on the rate at which the aging occurs. In order to attempt to determine which aging conditions had the largest effect, the internal resistance curves for batteries of similar aging conditions were isolated. The results are displayed in Figure 39, Figure 40, and Figure 41

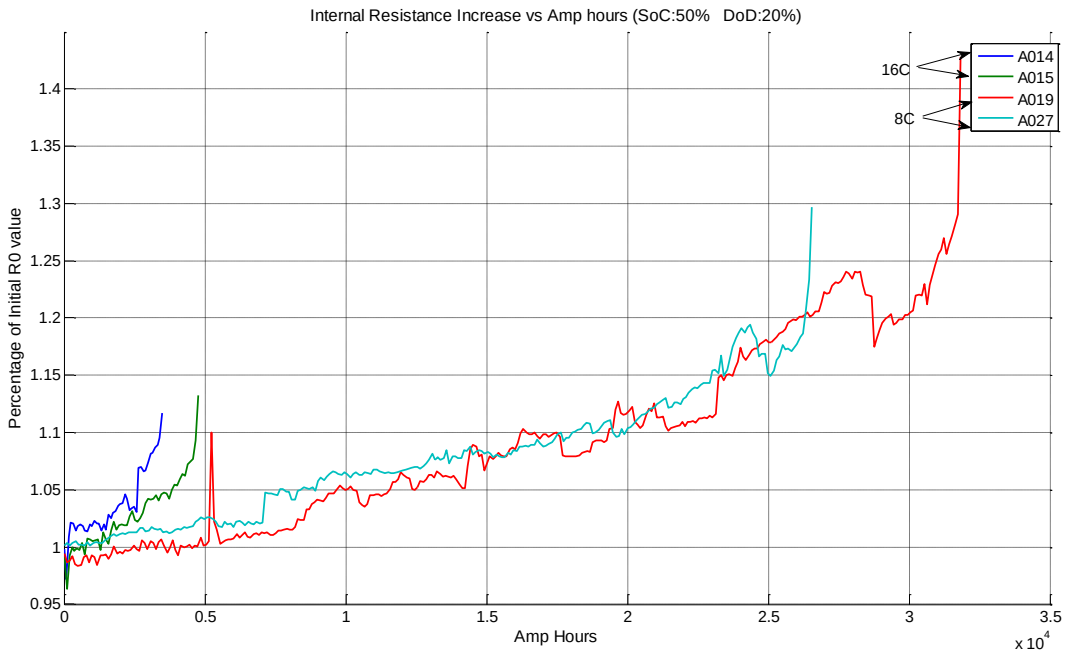

Figure 39: Internal Resistance curves for batteries aged at 50% SOC and 20% DOD

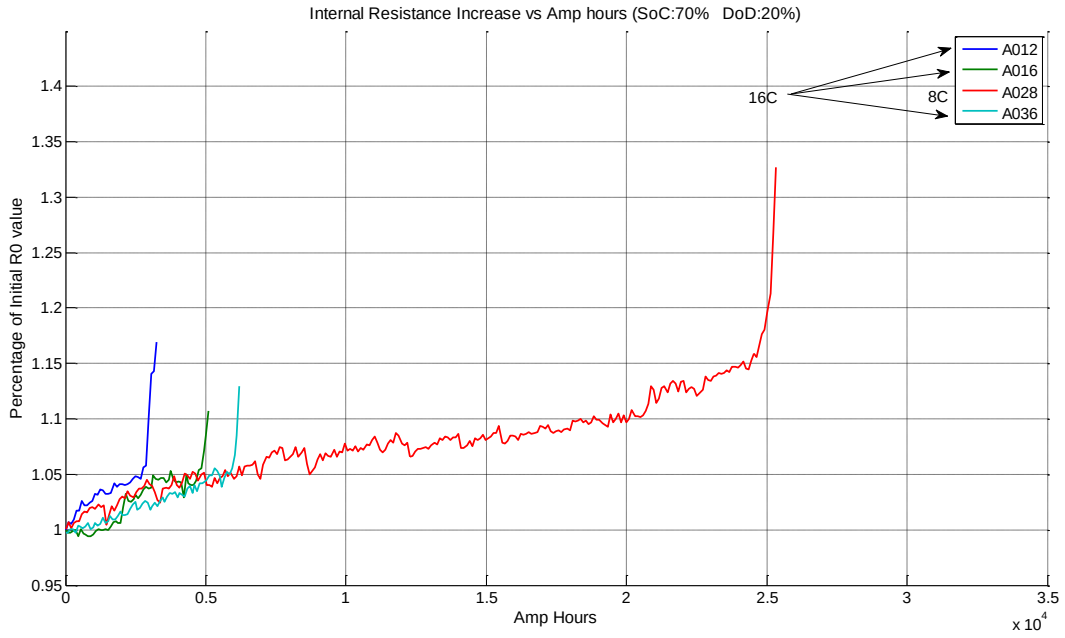

Figure 40: Internal Resistance curves for batteries aged at 70% SOC and 20% DOD

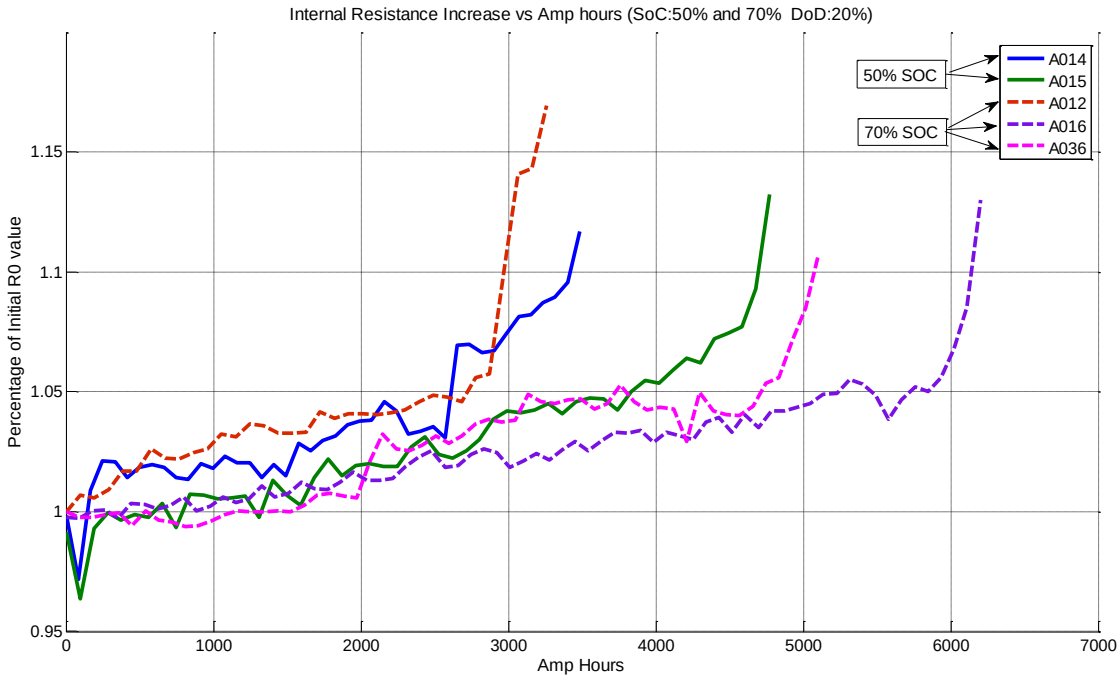

Figure 41: Internal Resistance Curves for Batteries aged at 70% and 50% SOC

The largest trend, as evidenced by Figures 40 and 41, is that the C-rate a battery was aged at had the largest impact on how long the battery lasted. Operating batteries at half the C-rate effectively increased their lifespan by five times. Considering batteries aged at the same C-rate, but different states of charge as in Figure 41 yielded little information. From Figure 38, it appeared batteries aged at 30% SOC died quickly but besides that, there were no other obvious relationships such as the correlation between lifespan and C-rate seen in the previous figures. Further analysis would be necessary to uncover any subtler relationships between rate of aging and aging conditions such as state of charge and depth of discharge.

CHAPTER 5

CONCLUSION

In conclusion, the quantification of aging of lithium ion batteries was accomplished by fitting relatively simple dynamic battery models at various stages of aging in the lives of batteries. The dominant parameter that showed the most correlation with aging was the zeroeth order internal resistance component, R_0. Therefore, the need to pursue a more sophisticated higher order model was not warranted. Because only the change in internal resistance was monitored, a less complex identification scheme was used to approximate resistance every time a step change in current was observed. This method of resistance tracking and calculation would lend itself well to applications onboard a vehicle. In this setting, resistance estimation would take place in real time, every time the battery experienced a change in current.

Different scenarios of aging were investigated, where temperature was held constant and state of charge, depth of discharge, and current rates varied across the set of batteries. Trends in the growth of internal resistance were identified with regard to the severity of the conditions under which a battery was aged. Resistance growth was quasi-linear for the majority of battery life and increased exponentially at the end of life.

Although a statistical dispersion was evident, the slope of linear resistance growth depended on the severity of that battery's aging conditions.

These observations regarding the growth of internal resistance should be the basis for my future work as a graduate student in the area of battery aging. Although it was not included in this report, initial analyses on the relation of resistance growth to capacity loss have been performed which indicate a strong relationship exists between the increase of resistance and decrease of capacity. This relationship will allow for the development of diagnostic and prognostic algorithms that unobtrusively estimate the current total capacity of a battery and predict the amount of useful life remaining before the battery reaches end of life.

BIBLIOGRAPHY

1. "EIA - International Energy Outlook 2008-World Energy Demand and Economic Outlook." *Energy Information Administration - EIA - Official Energy Statistics from the U.S. Government.* June 2008. 08 Apr. 2009 <http://www.eia.doe.gov/oiaf/ieo/world.html>.
2. Serrao, L., Onori, S., Guezennec, Y. and Rizzoni, G., *Model Based Strategy for Estimation of the Residual Life of Automotive Batteries*, Proc. of Safeprocess '09 Conference, Barcelona, Spain, July 2009.
3. J. Axen, A. Burke and K. Kurani, *Batteries for Plug-In Hybride Electric Vehicles (PHEV's): Goals and the State of Technology circa 2008*, Institute of transportation – University of California, May 2008
4. D. Sauer and H. Wenzl, *Comparison of different approaches for lifetime prediction of electrochemical systems – Using lead acid batteries as example*, Journal of power sources 176 534-546, 2008
5. B. Liaw and M. Dubarry, *From Driving cycle analysis to understanding battery performance in real-life electric hybrid vehicle operation*, Journal of power sources 174 76-88, 2007

6. Hu, Y., Yurkovich, B. J., Yurkovich, S and Guezennec, Y., *Electro-Thermal Battery Modeling and Identification for Automotive Applications*, Proc. of the 2009 Dynamic Systems and Control Conference (DSCC'09), Hollywood, CA, October 12-14, 2009.
7. Madella, N., Neal, J., Onori, S., and Guezennec, Y., *Aging Duty Cycle Extraction and Methodology for Laboratory Aging*. Columbus: The Ohio State University Center for Automotive Research, 2009.
8. United States. Department of Energy. *FreedomCAR Battery Test Manual for Hybrid Electric Vehicles*. United States Council for Automotive Research, Oct. 2003. Web. June 2009. <http://www.uscar.org/guest/view_team.php?teams_id=11>.